iScience

Article

Single-nucleus profiling of Ossabaw pig atherosclerosis model

Graphical abstract

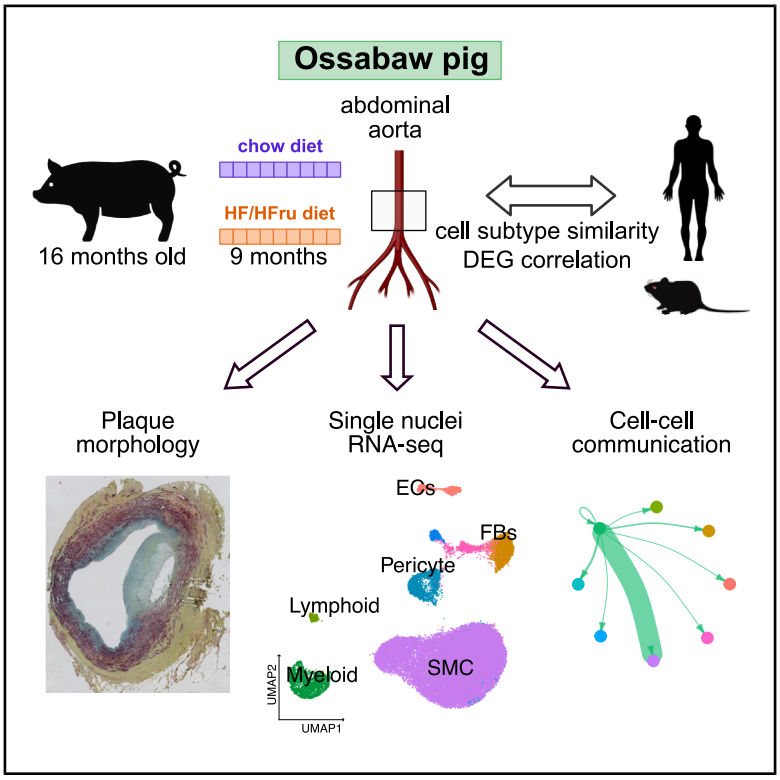

Highlights

- Ossabaw minipig as a preclinical model for human atherosclerosis with plaque calcification
- snRNA-seq of 36k+ nuclei from pig aortas on atherogenic vs. chow diets
- Found phenotypic switches in vascular smooth muscle and immune cells in atherosclerosis
- Integrated 4 human and 2 mouse scRNA-seq datasets for pig atherosclerosis comparison

Authors

Olga Bondareva, Marlene Hausner, Manuela Konert, ..., Peter M.H. Heegaard, Bilal N. Sheikh, Sabine Steiner

Correspondence

olga.bondareva@helmholtz-munich.de

In brief

Porcine; Transcriptomics; Model organism; Cardiovascular medicine

Bondareva et al., 2025, iScience *28*, 113464
October 17, 2025
https://doi.org/10.1016/j.isci.2025.113464

CellPress

iScience

CellPress
OPEN ACCESS

Article

Single-nucleus profiling of Ossabaw pig atherosclerosis model

Olga Bondareva,[1,2,9,*] Marlene Hausner,[1,2] Manuela Konert,[1,2] Daniela Branzan,[1,3] Katharina Noreikat,[4] Susann Oßmann,[5] Levani Sopromadze,[2] Antonia Geisler,[6] Peter M.H. Heegaard,[7] Bilal N. Sheikh,[1] and Sabine Steiner[1,2,8]

[1]Helmholtz Institute for Metabolic, Obesity and Vascular Research (HI-MAG) of the Helmholtz Center Munich at the University of Leipzig and University Hospital Leipzig, Leipzig, Germany
[2]Division of Angiology, Department of Internal Medicine, Neurology and Dermatology, University Hospital Leipzig, Leipzig, Germany
[3]Clinic and Policlinic for Vascular and Endovascular Surgery, School of Medicine and Health of the Technical University of Munich, Munich, Germany
[4]Medical-Experimental Center, University of Leipzig, Medical Faculty, Leipzig, Germany
[5]University Hospital for Heart Surgery, Heart Center Leipzig, Leipzig, Germany
[6]Department of General, Visceral and Transplant Surgery, University Hospital Graz, Graz, Austria
[7]The European Ossabaw Facility, DTU Health Technology, Technical University of Denmark, Kgs. Lyngby, Denmark
[8]Department of Internal Medicine II, Division of Angiology, Medical University Vienna, Vienna, Austria
[9]Lead contact
*Correspondence: olga.bondareva@helmholtz-munich.de
https://doi.org/10.1016/j.isci.2025.113464

SUMMARY

Atherosclerosis is a major cause of cardiovascular disease, and accurate preclinical models are essential for developing effective therapies. The Ossabaw pig model has high potential due to its physiological similarity to humans, but its molecular characterization remains limited. To address this, we performed single-nucleus RNA sequencing of over 36,000 nuclei from aortas of Ossabaw pigs fed chow or atherogenic diets. Our analysis revealed activation of brain-derived neurotrophic factor (BDNF), transforming growth factor β (TGF-β), SPP1, and interleukin-2 (IL-2) signaling pathways in atherosclerosis, along with smooth muscle cell transitions to synthetic and pro-osteogenic states, endothelial-to-mesenchymal transition, and TREM2+ immune cell phenotypes. Advanced fibrotic, immune cell-infiltrated plaques with calcification sites paired with molecular changes closely resembled those seen in human atherosclerosis. Together, our findings establish the Ossabaw pig as a valuable translational model and provide high-resolution data to support its use in preclinical cardiovascular research.

INTRODUCTION

Cardiovascular diseases (CVDs) are the leading cause of death worldwide, representing more than 30% of all deaths.[1,2] Atherosclerosis—accumulation of lipids in vascular walls with subsequent vessel occlusion and reduction of blood flow (stenosis)—is the main underlying cause of CVD. Atherosclerosis-triggered changes lead to conditions like ischemic heart disease, stroke, and peripheral arterial occlusive disease. While lifestyle changes and guideline directed pharmacotherapy, particularly lipid-lowering drugs, are crucial for prevention,[3] revascularization may be necessary in advanced cases, with minimally invasive endovascular treatments and specialized devices developed to improve acute and long-term outcomes.

Pig models are widely accepted for studying human disease, especially in the cardiovascular system.[4–6] The similarity of pig's anatomy and physiology, such as heart size, heart rate, omnivorous diet, and genomic similarity to human, recapitulates human vascular system better than rodent models and allows for more accurate experimental conclusions.[7,8] Diet-induced pig models of atherosclerosis can develop complex atherosclerotic lesions with formation of lipid-rich cores, fibrous caps, and calcifications that mimic human atherosclerosis,[9–12] without the need for genetic mutations such as *Apoe* or *Ldlr* deletions used in rodent models. Moreover, the vessel diameter in pigs is comparable to humans, which makes them suitable for testing of endovascular treatments and devices,[7,13,14] stent implants, and restenosis studies,[15] facilitating quicker translation to clinical studies. The use of minipigs is preferred to larger swine models due to animal size, housing conditions, and financial expenses. In this regard, the Ossabaw minipig is an ideal model, where adult minipigs reach sexual maturity and the average weight of adult human (70–80 kg) at around 6 months of age.[7] Ossabaw pigs are genetically predisposed to obesity even on normal chow diet,[7,16,17] while specialized high-caloric high fat/high fructose (HF/HFru) diet accelerates the development of metabolic syndrome and hypercholesterolemia.[18,19] Moreover, they were shown to develop atherosclerotic lesions and calcifications of coronary arteries,[18,20,21] making them a suitable model for preclinical cardiovascular research.

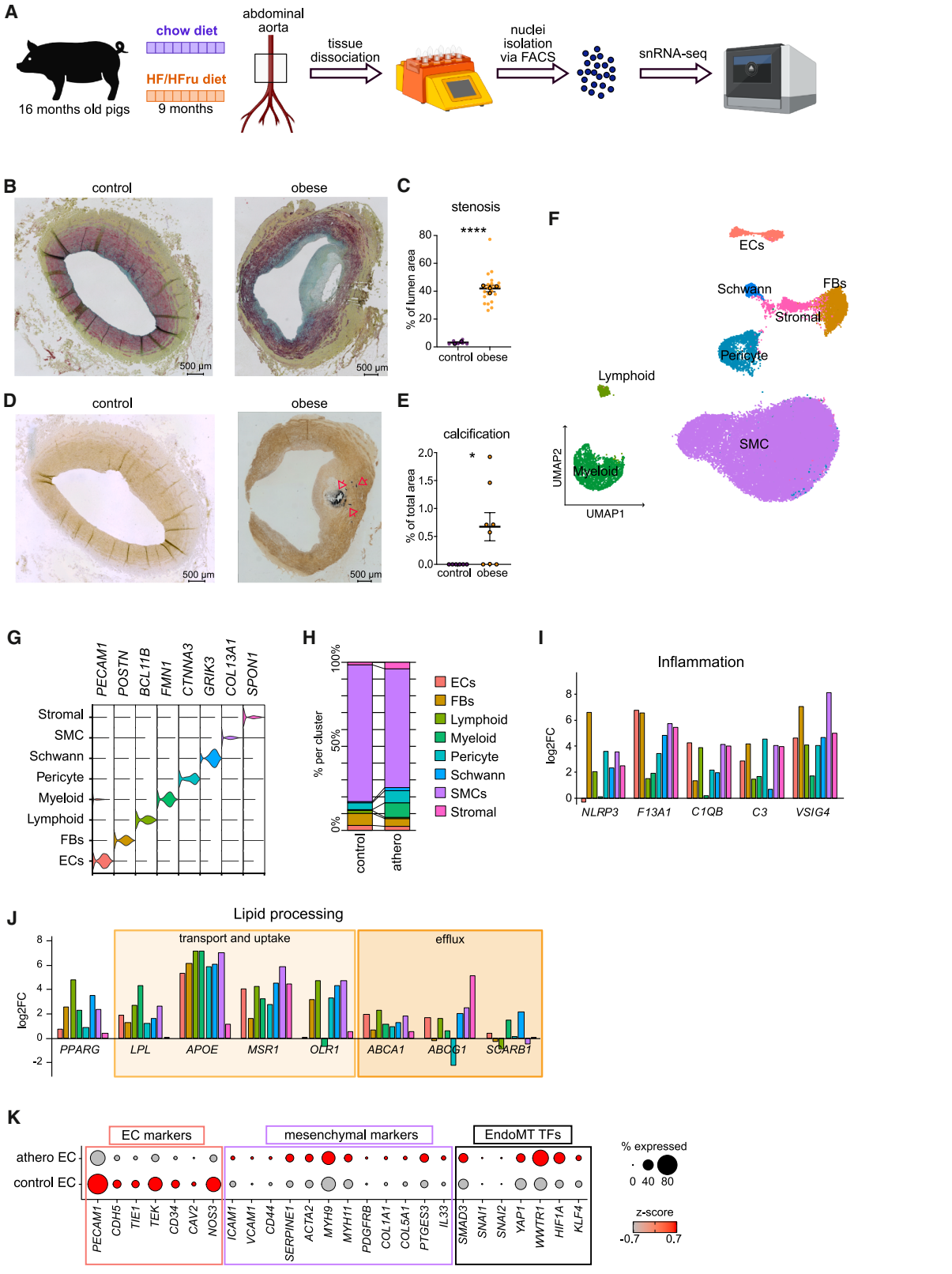

(legend on next page)

Despite multiple benefits of using pig models for cardiovascular research, prior studies have also highlighted inconsistencies between porcine and human data. Interventional devices such as stents have shown different efficacies in preclinical pig models versus human clinical studies,[22] most likely due to differences in atherosclerosis progression and healing processes. However, a systematic molecular evaluation between atherosclerosis development in the pig versus human is yet to be undertaken. A thorough understanding of potential similarities and differences in atherosclerotic plaque composition and response to injury between species is essential for improving efficacy of translational research.

In this study, we leverage single-cell technologies to characterize the atherosclerotic process in the Ossabaw minipig model to facilitate basic and preclinical research. We observed advanced atherosclerotic plaques with calcification in abdominal aortas of obese Ossabaw pigs. Single-nucleus RNA sequencing (snRNA-seq) analysis identified all major aortic cell types including infiltrating immune cells and foamy macrophages (MFs), observed phenotypic switches in vascular smooth muscle, immune and endothelial cells (ECs), and characterized signaling pathways and intercellular communication networks impeded by atherosclerosis. Through comparisons with atherosclerotic changes reported in mice and human, we report that the Ossabaw pig is a suitable model for preclinical research due to the similarity of both morphological and molecular changes to human disease.

RESULTS

Ossabaw pigs develop obesity and atherosclerosis following obesogenic diet

In order to characterize the Ossabaw pig for CVD studies, we utilized dietary induction of atherosclerosis with a high-fat and high-fructose diet (HF/HFru). Castrated male pigs of 16-month age were put on an HF/HFru or chow diet for 9 months (Figure 1A). Animals on HF/HFru diet became obese with an approximately 2-fold increase in weight at the end of the treatment (Figure S1A, $p < 10^{-3}$), as well as increased low-density lipoprotein (LDL) plasma levels compared to their chow-fed counterparts (Figure S1B, $p = 0.04$).

We retrieved samples from abdominal aortic regions between renal and iliac arteries branching points for histological and molecular characterization. Histological analyses confirmed the formation of fibrous cap atheromas and fibrocalcific plaques in obese pigs (Figures 1B and S1C–S1E) based on the classification system typically used for human atherosclerosis.[23] We observed pathological thickening of intima (blue), formation of necrotic core (light blue), degradation of internal elastic membrane, medium transformation (red), and lipid accumulation (Figures 1B and S1C–S1E). Quantification of intima and media thickness showed a significant increase of these features in obese animals compared to controls (Figures S1F and S1G, $p < 10^{-4}$). Average lumen reduction due to plaque formation measured 42% in obese pigs, corresponding to moderate stenosis, compared to 3% in lean animals (Figure 1C, $p < 10^{-4}$). Moreover, all obese pigs developed plaque calcification in aortas, on average 0.67% of total section area, as evident by von Kossa silver staining (Figures 1D–1E, $p = 0.04$; Figure S1D, red arrows).

Together, these histological analyses revealed classical characteristics of atherosclerosis including increased intima and media, stenosis, lipid accumulation, and calcification.

snRNA-seq uncovers hallmarks of atherosclerotic plaques in pig aortas

Having confirmed atherosclerotic status of obese pig aortas, we performed snRNA-seq on 3 atherosclerotic and 2 control aortic samples and integrated the data (Figures 1F and S2). After filtering, we performed quality control checks (Figure S2). Ribosomal and mitochondrial transcript count was less than 1%, while the median genes detected per cell varied between 500 and 4,000, highlighting the high quality of our data. Following integration, we obtained a total of 36,209 nuclei for further analysis. We identified major vascular cell types based on the conventional cell type markers: ECs (*PECAM1*, *FLT1*, and *NOS3*), fibroblasts (FBs) (*POSTN*, *DCN*, and *STK32B*), smooth muscle cells (SMCs) (*PCDH7*, *ACTA2*, *MYH11*, and *COL13A1*), pericytes (*CTNNA3*, *RGS6*, and *PDGFRB*), Schwann cells (*GRIK3* and *XKR4*), stromal cells (*SPON1* and *SCARA5*), myeloid (*PTPRC*, *MSR1*, *DOCK4*, and *FMN1*), and lymphoid cells (*BCL11B*, *SKAP1*, and *IKZF1*) (Figures 1G, S3A, and S3B). Each cell type was identified in each pig sample (Figure S2F), allowing us to undertake detailed analyses of cell types in obese versus control samples.

Inflammation is a key hallmark of atherosclerosis. We observed an 18-fold increase in myeloid cell numbers in aortas of obese samples, supporting the presence of advanced atherosclerotic plaques (Figures 1H, S3C, and S3D). Strong upregulation of inflammatory genes was evident in all cell types, including inflammasome (*NLRP3*) and complement system activation (*F13A1*, *C1QB*, *C3*, and *VSIG4*) (Figure 1I). As typical for human atheroma,[24] all cell types displayed an upregulation of genes involved in nuclear lipid

Figure 1. Characterization of HF/HFru diet-induced changes in aortas of Ossabaw minipigs

(A) Schematic design of the experiment.

(B and D) Representative histological staining of aortic samples (B) with Movat pentachrome-modified Russell-Movat staining (blue, intima; red, media; yellow, adventitia) and (D) with von Kossa silver staining; black, calcium deposits. Scale bar, 250 μm.

(C) Quantification of vessel stenosis, percentage of plaque to total lumen area. Pale dots represent technical replicates, and outlined dots represent biological replicates, i.e., mean of technical replicates per each animal, p values < 0.0001, Mann-Whitney test.

(E) Calcification quantification as a percent of total vessel area, p value = 0.04, unpaired Student's t test.

(F) Uniform manifold approximation and projection (UMAP) of the snRNA-seq data from combined control and atherosclerotic pig aortas.

(G) Violin plot of cell type-specific marker gene enrichment per cluster.

(H) Stack plot showing percentage of cells in each cluster provided from control or atherosclerotic samples.

(I and J) Bar plot showing log2 fold change in atherosclerotic samples of (I) inflammation-associated genes and (J) lipid-processing genes in each cluster.

(K) Dot plot of genes related to EndoMT in endothelial cells. Dot size indicates the percentage of cells expressing gene of interest, and color indicates z-score of the average expression level.

sensing (*PPARG*), lipid transport and uptake (*LPL*, *APOE*, *MSR1*, and *OLR1*), and cholesterol efflux (*ABCA1*, *ABCG1*, and *SCARB1*) (Figure 1J). This transcriptional change was in line with high lipid content in diseased aortas (Figure S1C).

ECs in atherosclerosis undergo endothelial-to-mesenchymal transition (EndoMT).[25–28] In the Ossabaw pig, we also observed activation of EndoMT in atherosclerotic samples, but not in controls (Figure 1K). ECs reduced expression of canonical endothelial markers (*PECAM1*, *CDH5*, *TIE1*, and *TEK*) and nitric oxide synthase (*NOS3*), while upregulating mesenchymal and SMC markers (*S100A4*, *ACTA2*, *MYH9*, *MYH11*, *COL1A1*, *PTGES3*, and *IL33*) and transcription factors associated with disturbed flow and EndoMT (*SMAD3*, *SNAI1*, *SNAI2*, *YAP1*, *WWTR1*, *HIF1A*, and *KLF4*)[25,28,29] (Figure 1K).

Together, these data show that Ossabaw pigs develop obesity and aortic atherosclerosis after 9 months of an obesogenic HF/HFru diet supported by inflammatory, lipid metabolism, and EndoMT transcriptomic signatures.

Multiple cell types contribute to extracellular matrix reprograming, lipid metabolism, and inflammation in atherosclerosis

To identify the transcriptional changes in atherosclerotic aortas, we performed differential expression analysis on each cell type. SMCs were the most affected cell type, with ~3,500 differentially expressed genes (DEGs) in atherosclerotic versus control samples, followed by ECs, FBs, and myeloid cells (Figure 2A; Table S3). DEGs across cell types displayed relatively high correlation (Figure 2B), suggesting that some common pathways may be affected across all cell types in atherosclerosis. For instance, genes upregulated across all cell types included osteopontin (*SPP1*), Shisa homolog 9 (*SHISA9*), and cytochrome P450 family 7 subfamily A member 1 (*CYP7A1*), which are involved in metabolism of endogenous cholesterol, as well as mucolipin 3 (*MCOLN3*), sphingomyelin phosphodiesterase acid like 3A (*SMPDL3A*), and matrix metalloproteinase 9 (*MMP9*) (Figures 2C and S4A). Gene ontology (GO) analysis revealed an upregulation of transforming growth factor β (TGF-β) regulation of extracellular matrix, pro-inflammatory brain-derived neurotrophic factor (BDNF)[30] signaling, and interleukin-2 (*IL-2*) signaling pathways in most cell types (Figure 2D). This indicates that multiple cell types contribute to the overall increase in cholesterol processing, calcification, and remodeling in Ossabaw pig atherosclerosis.

In contrast to upregulated genes, common downregulated genes included stearoyl-coenzyme A desaturase 5 (*SCD5*), *CD34*, and homeobox A2 (*HOXA2*) (Figures 2E and S4B). GO analysis of downregulated genes showed an enrichment of lipid metabolism-related terms in pericytes, SMCs, and stromal cells, as well as downregulation of cell migration and adhesion via integrin signaling and natural killer cell-related pathways in lymphocytes (Figure 2F). Thus, we identified evidence for pro-inflammatory and pro-fibrotic signatures across multiple cell types in atherosclerotic samples.

SMCs switch to pro-osteogenic and pro-inflammatory phenotypes

To understand phenotypic switches in atherosclerosis, we subclustered SMCs, ECs, and immune cells based on their transcriptional profiles. SMCs clustered into 4 subpopulations: *ACAA2*$^+$ SMC_1, *SPP1*$^+$ SMC_2, *NFATC2*$^+$ SMC_3, and *TRPC4*$^+$ SMC_4 (Figures 3A–3C and S5A). To uncover functional networks active in each SMC cluster, we performed GO enrichment analysis on genes significantly enriched in each SMC subpopulation. SMC_1 and SMC_4 exhibited housekeeping functions such as mitochondrial respiration and control of vascular tone (Figure S5A), and SMC_1-specific genes were enriched in calcium signaling pathway (Figure S5B), while SMC_4 displayed enrichment in cholesterol and steroid biosynthesis networks (Figure S5C). SMC_4 nuclei were also enriched in genes associated with axon guidance (Figure S5D). Clusters SMC_2 and SMC_3 were associated with the pro-inflammatory BDNF signaling pathway (Figure S5E). SMC_2 and SMC_3 showed upregulation of AP-1 transcription factor subunits *JUN*; *JUNB*; *FOSB*; anti-proliferative genes *BTG1* and *DUSP1*; and stress-activated genes *HSPA8*, *HSPB1*, *TRAF3IP2*, and *ATF3*.

Comparison of 4 SMC cluster fraction in atherosclerotic versus control aorta samples showed that SMC_1 and SMC_4 clusters were mostly composed of nuclei from aortas of control animals (89.4% and 90.1%, respectively). In contrast, SMC_2 and SMC_3 were primarily found in atherosclerotic aortas (91.2% and 96.7%, respectively) (Figure 3B). Based on marker gene expression, the SMC_1 subcluster was the most similar to contractile SMCs, and cells in SMC_2 cluster expressed markers of both contractile and activated SMCs, while SMC_3 and partially SMC_4 cells were most similar to synthetic SMCs. Activated SMC_2 expressed markers of both pro-osteogenic (*SPP1* and *IBSP*[31–33]) and pro-inflammatory (*TREM2*, *CD163*, and *MSR1)* phenotypes. *RUNX2*[34] and *KLF4*,[34,35] two transcription factors promoting osteoblast differentiation and calcification of atherosclerotic plaques, were enriched in the SMC_3 population, suggesting their transitional state toward osteoblast-like phenotypes. Synthetic SMC_3 expressed lower levels of *ACTA2* and *MYH11*, while upregulating *FN1*, *COL1A1*, *PDGFRA*, and *TCF21*, supporting their switch to synthetic, fibromyocyte-like phenotype (Figure 3C).[36–38] These data suggest a broad shift in SMC phenotypes from a healthy contractile state (SMC_1) to activated pro-osteogenic pro-inflammatory (SMC_2) and synthetic fibromyocyte-like phenotypes (SMC_3).

To further uncover the atherosclerosis-specific transcriptional signature in SMCs, we performed differential gene expression analysis on SMC clusters enriched in atherosclerosis (i.e., SMC_2 and SMC_3), versus SMC clusters enriched in control animals (i.e., SMC_1 and SMC_4). Gene set enrichment analysis (GSEA) of DEGs revealed upregulation of collagen biosynthesis and chondrocyte development processes (Figure 3D) and downregulation of various metabolic processes, including cellular lipid metabolic process and fatty acid catabolism in atherosclerosis-enriched clusters (Figure 3E).

Together, these data further support the phenotypic switch of SMCs to synthetic, pro-inflammatory and pro-osteogenic phenotypes in atherosclerosis.

ECs display an inflammatory phenotype and activation of coagulation networks in atherosclerosis

ECs clustered into 4 subpopulations, with *LTBP2*$^+$ EC_2 being mostly represented by control nuclei (98.5%), while EC_1 and

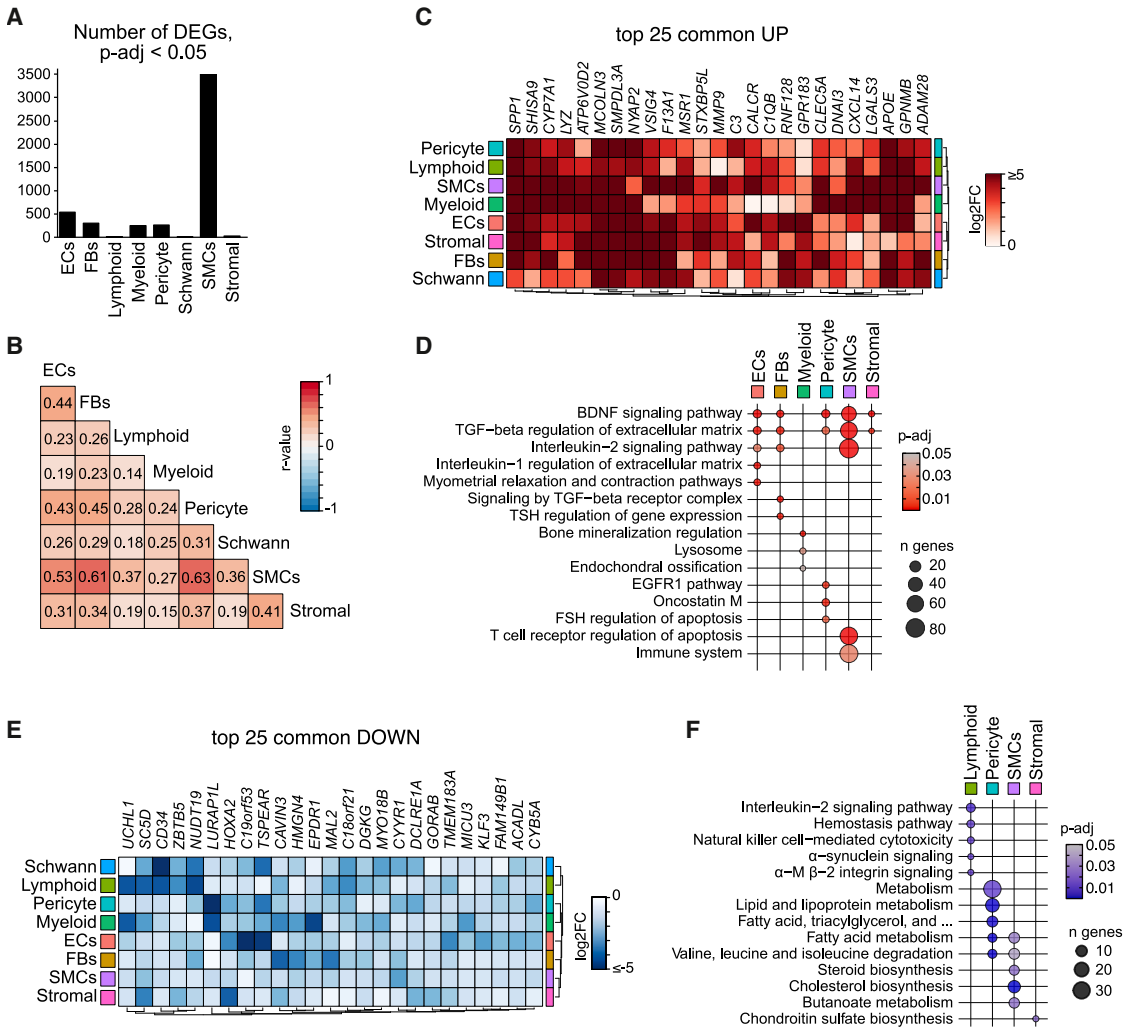

Figure 2. Atherosclerosis-induced changes in gene expression across vascular cell types

(A) Number of DEGs per cell type in atherosclerosis.

(B) Correlation of significant DEGs between cell types. Numbers indicate Pearson's correlation coefficient (R value).

(C) Top 25 upregulated genes across all cell types, log2 fold change.

(D) Dot plot of GO terms enriched in upregulated genes. Dot size indicates the number of genes found in the GO term, and color indicates the Benjamini-Hochberg adjusted *p* value of enrichment.

(E) Top 25 downregulated genes across all cell types, log2 fold change.

(F) Dot plot of GO terms enriched in downregulated genes. Dot size indicates the number of genes found in the GO term, and color indicates the Benjamini-Hochberg adjusted *p* value of enrichment.

CA10^{+} EC_4 had higher content of atherosclerotic nuclei (77.5%) (Figures 3F, 3G, and S5F). Based on the expression of arterial and vasa vasorum markers,[39–41] EC_1 and EC_4 appear to be derived from the vasa vasorum EC pool, while EC_2 and EC_3 represent intimal ECs of aorta (Figures 3H and 3I).

GO analysis performed on cluster-specific genes revealed enrichment in angiogenesis and vascular endothelial growth factor (VEGF) pathways in a bi-modal pattern (Figure S5G). EC_1 and EC_4 expressed higher canonical VEGF signaling molecules, *MAGI1*, *VEGFC*, *FLT1*, *KDR*, and *CDC42*, and guanine nucleotide exchange factors *RASGRP3*, *RAPGEF4*, and *DOCK4*, related to actin reorganization and migration.[42] EC_2 and EC_3 expressed higher *VEGFA*, *BMX*, *TEK*, *PXN*, *SRC*, and *FGF2*, as well as phospholipase Cγ (*PLCG2*) and its downstream targets phospholipase A2 *(PLA2GA4)*, *PRKCA*, *RAF1*, and *NOS3* (Figure S5G). EC_4 showed increased expression of *PLCG1*, *PPP3CA*, and *NFATC2*, suggesting that EC_4 could promote prostaglandin I2 synthesis. EC_4 also displayed an upregulation of coagulation-related genes (Figure S5H) and purine metabolism-related genes (Figure S5I).

We next focused on functional categories enriched in each EC cluster. The EC_1 subcluster displayed high chemotaxis module score, implying their pro-inflammatory role in leukocyte adhesion

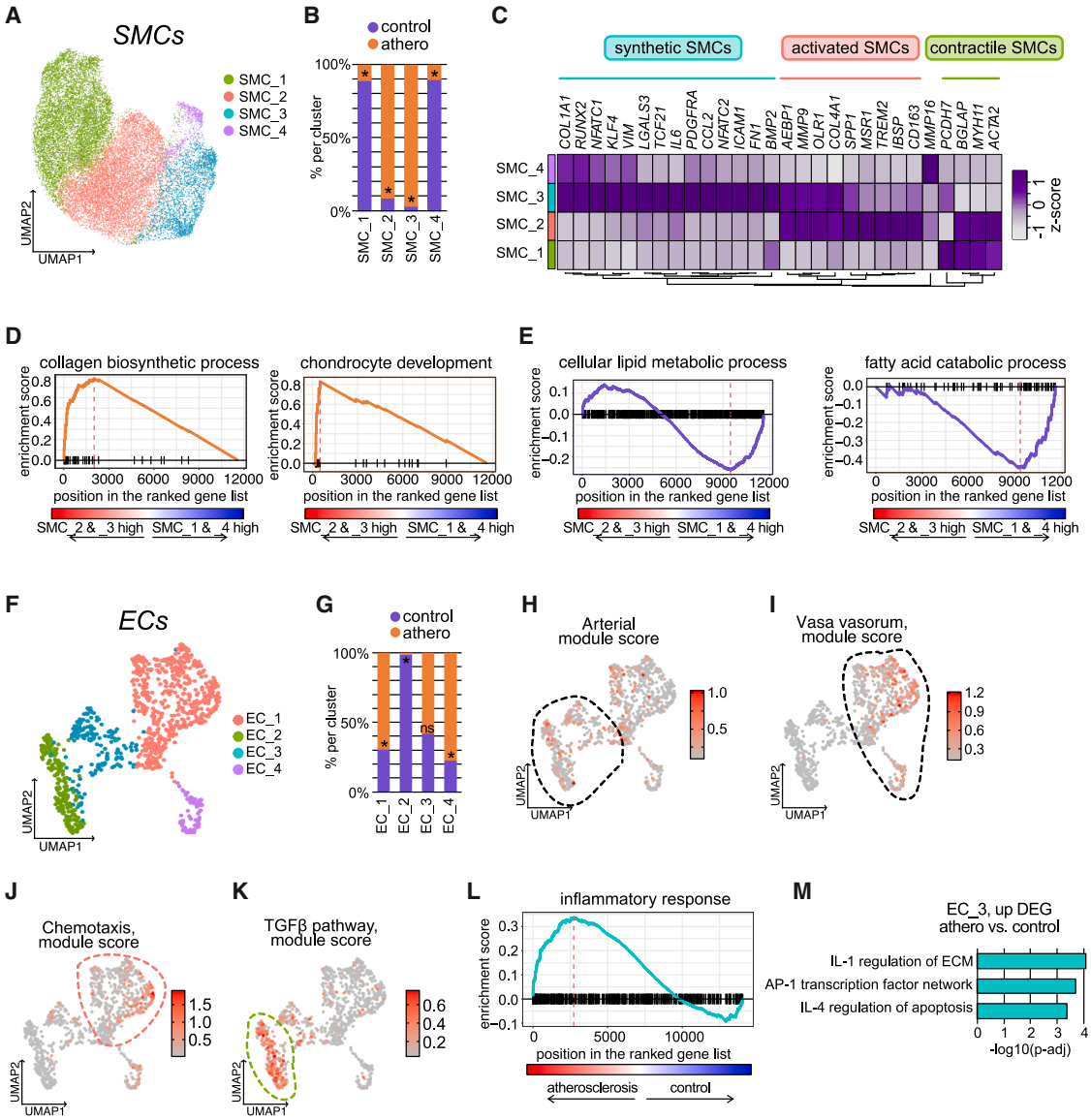

Figure 3. Subclustering and analysis of SMCs and ECs of aortas

(A) UMAP of subclustered SMCs.

(B) Distribution of cells per subcluster in each condition; χ^2 test; * indicates p values < 0.05.

(C) Heatmap showing Z score of genes specific for synthetic (blue), contractile (green), and activated (red) SMCs in each subcluster.

(D) GSEA plots of genes enriched in SMC_2 and SMC_3 versus SMC_1 and SMC_4 clusters.

(E) GSEA plots of genes enriched in SMC_1 and SMC_4 versus SMC_2 and SMC_3 clusters.

(F) UMAP of subclustered ECs.

(G) Distribution of cells per subcluster in each condition; χ^2 test; * indicate p values < 0.05.

(H) UMAP of arterial module score enrichment.

(I) UMAP of vasa vasorum module score enrichment.

(J) UMAP of chemotaxis module score enrichment.

(K) UMAP of TGF-β signaling pathway module score enrichment.

(L) GSEA plot of genes upregulated in EC_3 in atherosclerosis versus control.

(M) Selected top GO terms enriched in genes upregulated in EC_3 in atherosclerosis versus control. p-adj = Benjamini-Hochberg adjusted p value.

(Figure 3J). EC_2 was characterized by high TGF-β pathway activity (Figures 3K and S5J), with high relative expression of *TGFB2*, *SMAD2*, and *DAB2*, mediating c-Jun N-terminal kinase (JNK) activation. *CA10*, a member of the carbonic anhydrase family of zinc metalloenzymes, which catalyzes hydration of carbon dioxide, was strongly upregulated in the EC_4 population, while the expression of nitric oxide synthase 3 (*NOS3*) was significantly reduced (Figure S5K).

EC_3 cells were derived from the intima and showed similar proportions in atherosclerotic versus healthy aortas (Figure 3G). We identified DEGs in EC_3 and performed GSEA and GO analyses. These analyses revealed upregulation of immune response (Figure 3L), and enrichment of interleukins IL-1 and IL-4, and AP-1 pathways (Figure 3M), suggesting apoptotic and pro-inflammatory processes in intimal ECs in atherosclerosis.

Taken together, aortic ECs could be subclustered based on their physiological function (intimal and vasa vasorum ECs) and transcriptional programs, such as chemotaxis and TGF-β pathway activity. Moreover, activation of coagulation and pro-inflammatory processes were found in atherosclerosis.

Atherosclerotic samples display increased myeloid populations and foamy cell formation

We assessed atherosclerosis-associated changes in immune cell populations. Clustering identified 7 subpopulations, including B cells, T cells, four types of MFs, and progenitor-like cells (Figure 4A). B cells were mostly found in control samples (77%), while T cells were equally present in both (Figure 4B). T cells displayed an upregulation of transcriptional networks associated with p53 and PI3K-Akt signaling pathways, while natural killer (NK)-cell-mediated cytotoxicity and chemokine signaling pathways were downregulated (Figure 4C). Further subclustering of T cells revealed 5 subpopulations, including *CD4*$^+$ T cells, *CD4*$^+$ regulatory T cells, *OLR1*$^+$ T cells, *CD8*$^+$ T cells, and cytotoxic *CD8*$^+$ T cells, based on the expression of established markers[43] (Figures S6A–S6D). Interestingly, CD8$^+$ T cells were reduced, while T3 *OLR1*$^+$ T cells expressing oxidized low-density lipoprotein receptor 1 (*OLR1*) were increased in atherosclerotic samples (Figure S6E).

MFs were primarily detected in atherosclerotic samples (Figures 4B and S3C). We confirmed increased numbers of MFs via CD68 immunohistochemistry (Figures 4H and 4I). We could identify resident-like MF enriched in *CD163*, *LYVE1*, and other marker genes of both resident and pro-inflammatory MFs (Figures S6F and S6G). The second MF population was characterized by an increased SMC signature (Figures 4D and 4E), suggesting an SMC-like MF phenotype. Third and fourth MF clusters expressed triggering receptor expressed on myeloid cells-2 (*TREM2*) (Figure 4F). *TREM2*-expressing MF nuclei (*TREM2*$^+$ MF and foamy MF clusters) were enriched in genes associated with lysosome, sphingolipid, and glycosphingolipid metabolism (Figure 4G), indicating their involvement in processing of lipids accumulating in the plaque. The fourth MF cluster (foamy MF) had a strong foamy cell signature[44,45] (Figure S6I). Foamy MF nuclei displayed an enrichment of lysosome, platelet signaling networks, as well as insulin signaling and lipid metabolism (Figure S6J) compared to focal adhesion-related GOs in only *TREM2*$^+$ MF nuclei (Figure S6K).

Our analyses of the immune cell populations showed myeloid cell infiltration in atherosclerotic Ossabaw pig aortas with phenotypic switch of MFs to SMC-like and lipid-loaded foamy cells.

Pericytes and FBs show deregulation of metabolic and extracellular matrix genes

Other cell types that exhibited moderate transcriptional changes were pericytes and FBs (Figure 2A). In particular, downregulated genes in pericytes were enriched in β-oxidation of saturated fatty acids and lipid metabolism (Figures 4J and 4K). Similarly, FBs displayed downregulation of genes enriched in fatty acid and cholesterol metabolism and homeostasis, as well as actin cytoskeleton regulation (Figure 4L). Genes associated with BDNF pathway (AP-1 and stress response) and TGF-β regulation of the extracellular matrix (Figures 4M and 4N) were upregulated in pericytes and FBs in atherosclerotic samples, while IL-2 signaling was also increased in FBs.

Together, we uncovered heterogeneous populations of SMCs, ECs, and immune cells in atherosclerosis with strong upregulation of lipid-processing and foamy-like cell formation. Moreover, in the lesion, SMCs underwent phenotypic switch to synthetic, pro-inflammatory, and osteogenic fates, while MFs also shifted toward an SMC-like phenotype.

Atherosclerosis alters cellular communication in the aorta

Vascular homeostasis relies heavily on cell-cell communication within the vascular wall. We sought to identify changes in intercellular communication networks in atherosclerosis in the Ossabaw pig. We utilized the CellChat database[46] to determine the number and strength of predicted interactions between cell types based on gene expression profiles of ligands and receptors (Tables S4 and S5). FBs reduced the number of interactions with neighboring cells in atherosclerosis, which is likely due to the disintegration of the adventitia (Figures 5A and S6L). Meanwhile, myeloid cells increased the number of interactions, which could be explained by the infiltration of MFs into the lesion area (Figures 5A and S6L). Moreover, the interaction strength, defined by the level of expression of ligand-receptor pairs, showed an increase in myeloid-SMC, myeloid-pericyte, SMC-myeloid, SMC-pericyte, and SMC-Schwann cell interactions, while drastically decreasing in SMC-SMC communication (Figure 5B). The loss of SMC-SMC autocrine signaling was particularly striking. Majority of downregulated SMC-SMC interactions in atherosclerosis fell into the extracellular matrix (ECM)-receptor category, including multiple laminins, collagen 1A1, and tenascin-integrin interactions (Table S4), suggesting the reprogramming of the ECM in diseased aortas in response to injury.

To better identify global changes in communication modules across multiple cell types in atherosclerosis, we focused on the strongest signaling networks in the aorta. Control aorta cell interactions were represented by homeostatic signals such as *PECAM1*, *NRXN1*, *COL4A1*, *COL1A2*, *LAMC3*, and *FN1* (Figure 5C; Table S4). In contrast, cells from aortas of obese pigs activated cell-communication networks driven by osteopontin (*SPP1*), semaphorin 3C (*SEMA3C*), and transforming growth factor β 3 (*TGFB3*) (Figure 5D; Table S5). The main source of *SPP1* was myeloid cells, while strongest receiver receptors (*CD44*, *ITGAV*, *ITGA1*, *ITGA8*, *ITGA9*, *ITGB1*, and *ITGB5*) were expressed in SMCs (Figure 5E), confirming the presence of osteogenic stimuli in the plaque. Moreover, we observed increase in prostaglandin E2 (*PGE2*) signaling to SMCs in atherosclerotic aortas (Figure S6M). *PGE2* is an inflammatory mediator that can directly enhance osteoclast formation,[47,48] thus further promoting plaque calcification.

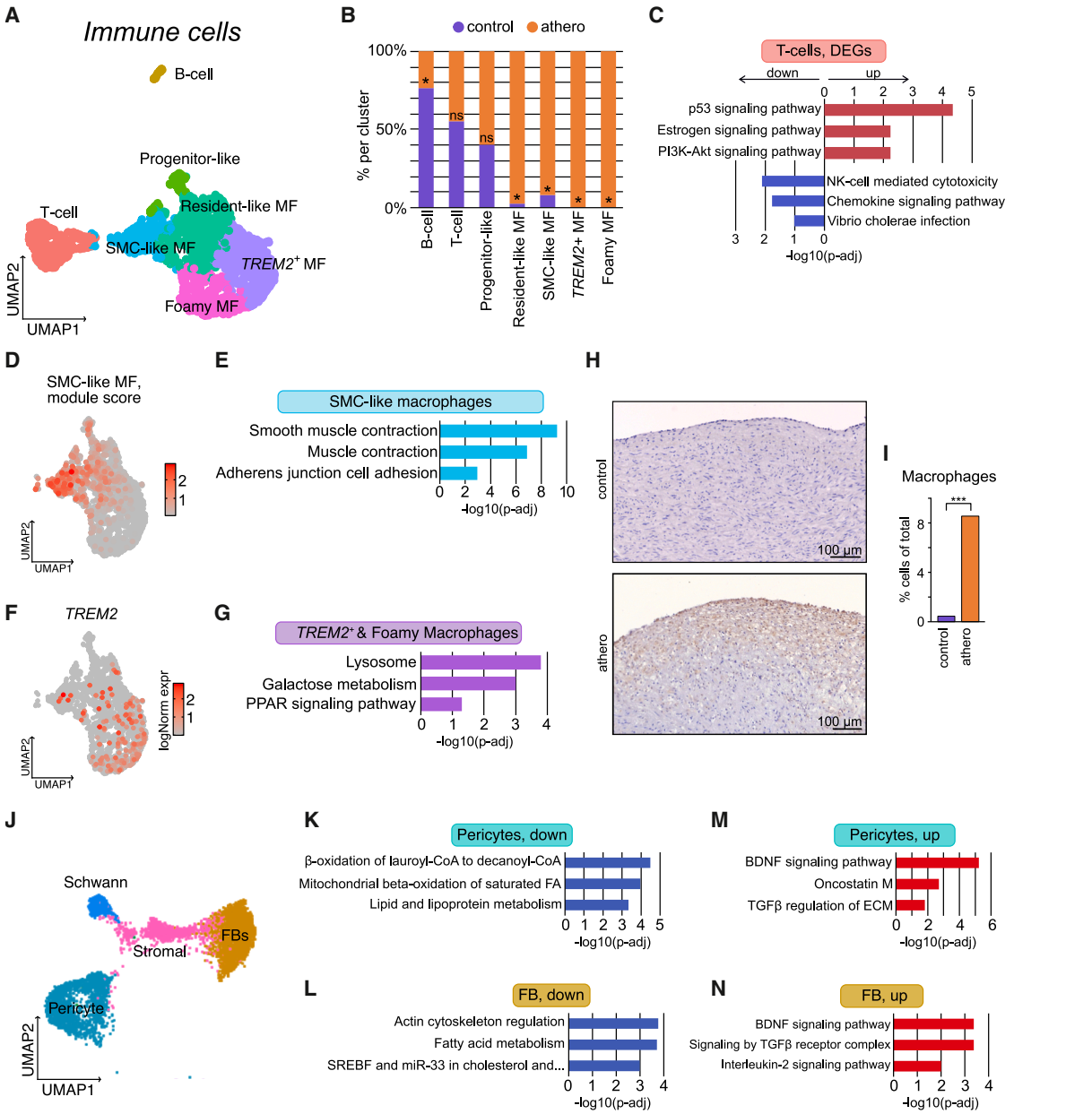

Figure 4. Subclustering and analysis of immune and other cell types of aortas

(A) Subclustering of immune cells.

(B) Distribution of cells per subcluster in each condition; χ^2 test; * indicate p values < 0.05.

(C) GO terms enriched in up- and downregulated genes of T cells.

(D) UMAP showing SMC-like signature module score.

(E) GO terms enriched in SMC-like macrophages.

(F) UMAP showing expression of *TREM2*.

(G) GO terms enriched in *TREM2*$^+$ and foamy MF subclusters.

(H) Representative immunohistochemistry images showing CD68$^+$ cells (pan-myeloid marker) in control and atherosclerotic aortas; scale bar, 100 μm.

(I) Bar plot of macrophage nuclus percentage in control and atherosclerosis snRNA-seq datasets; χ^2 test; *** indicate p values < 0.001.

(J) Subclustering of "other" non-EC, non-immune, and non-SMC cell types.

(K–N) GO terms enriched in (K) downregulated genes in pericytes, (L) upregulated genes in pericytes, (M) downregulated genes in FBs, and (N) upregulated genes in FBs. p-adj = Benjamini-Hochberg adjusted p value.

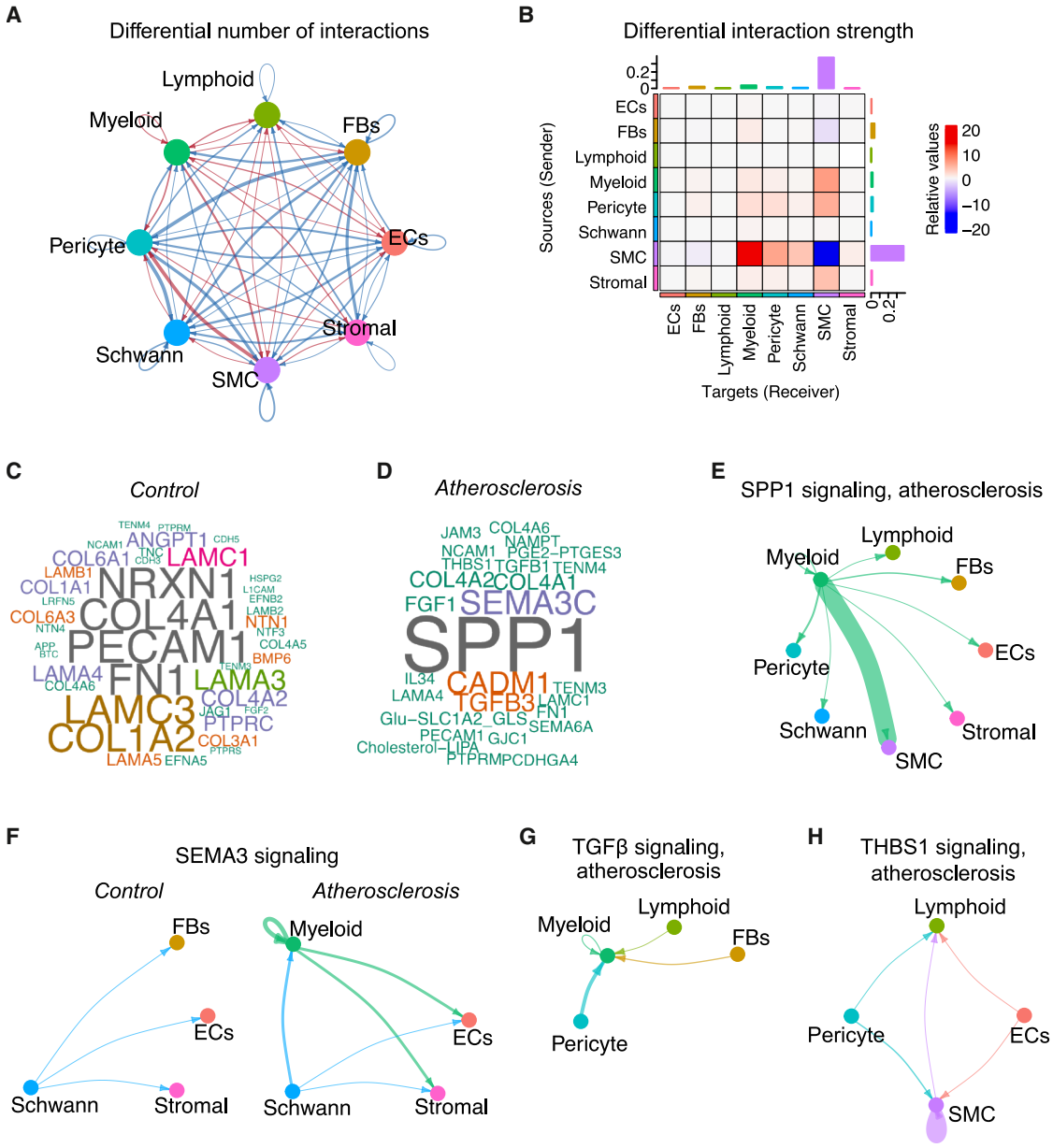

Figure 5. Cell-cell communication analysis of vascular cell types in atherosclerosis and control aortas

(A) Interaction plot of interactions between cell types changed in aortas of atherosclerotic vs. control aortas. Thickness of the lines represents the strength of interaction; blue, reduced interaction numbers; red, increased interaction numbers.

(B) Heatmap of interaction strength changes in atherosclerotic vs. control aortas.

(C and D) Word cloud representing most prevalent ligands in (C) control and (D) atherosclerotic conditions.

(E–H) Interaction maps showing (E) SPP1 signaling in atherosclerosis, (F) SEMA3 signaling in control and atherosclerotic samples, (G) TGF-β signaling in atherosclerosis, and (H) thrombospondin signaling in atherosclerosis. Thickness of the lines represents the strength of interaction.

Interestingly, semaphorin 3C (SEMA3C) was among the most dysregulated ligands (Figure 5F). In control conditions, it was signaling from Schwann cells to ECs, FBs, and stromal cells. In atherosclerotic samples, *SEMA3C* primarily signaled from Schwann to myeloid cells and from myeloid to ECs and stromal cells via the *NRP1*, *NRP2*, *PLXNA2*, and *PLXNA4* receptors (Figure 5F). While the role of SEMA3C in atherosclerosis in currently unknown, studies have reported *SEMA3C* association with obesity and insulin resistance[49] and adipose tissue fibrosis[50] in human.

TGF-β signaling networks were upregulated in atherosclerosis due to an increase in *TGFB1* and *TGFB3* from pericytes, FBs, and lymphoid cells. TGF-β signaling was communicated to myeloid cell via *TGFRB1*, *TGFRB2*, and *ACVR1* receptors

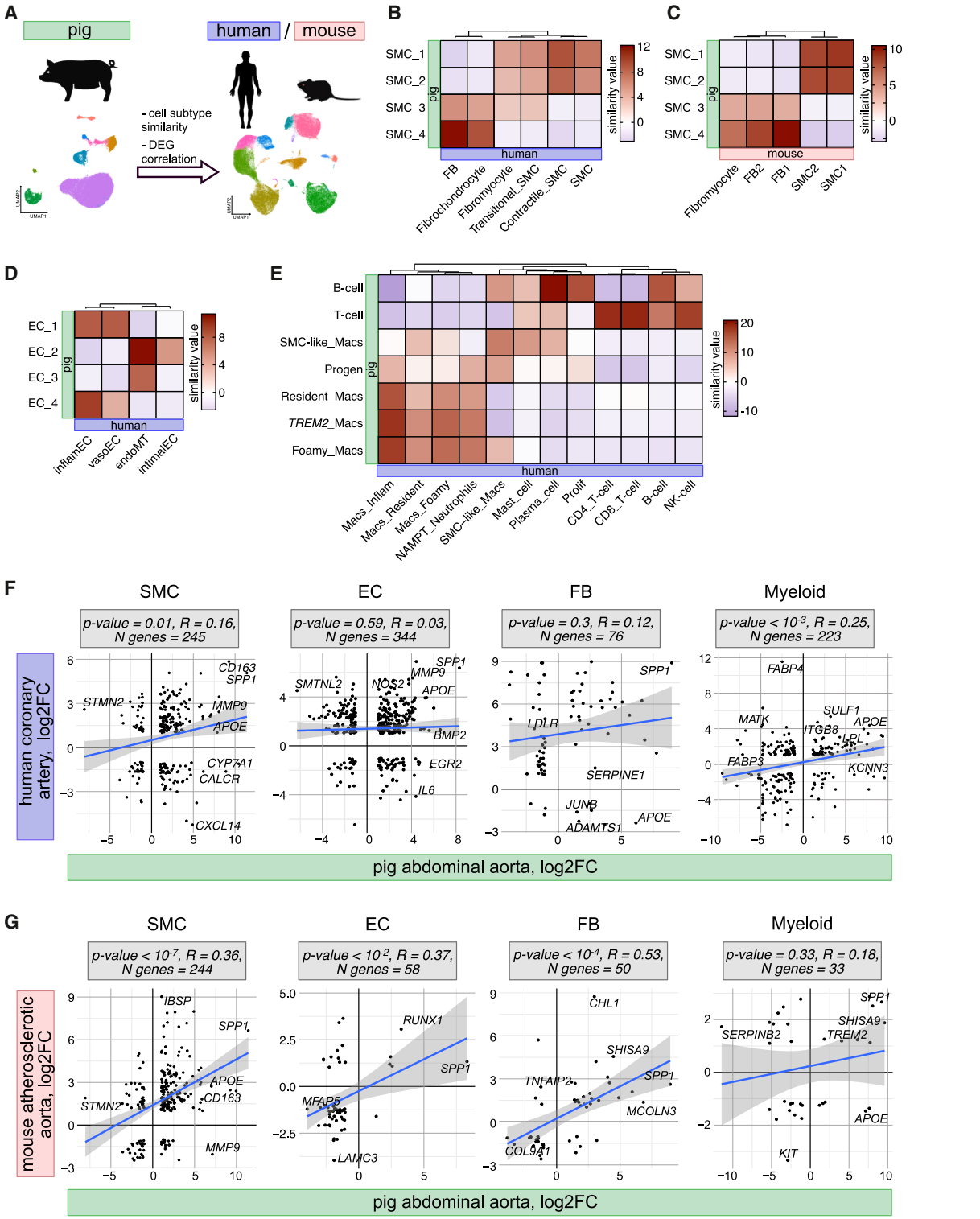

Figure 6. Comparison of Ossabaw pig SMC, EC, and immune subtypes and atherosclerosis-induced changes to humans and mice

(A) Schematic of inter-species comparison.

(B–E) Similarity heatmaps between pig abdominal aorta atherosclerosis snRNA-seq and integrated human atherosclerosis scRNA-seq datasets[37,55–57]: (B and C) SMC and FB subpopulations of (B) humans and (C) mice, (D) EC subpopulations, and (E) immune subpopulations.

(legend continued on next page)

(Figure 5G).[51] Similarly, we observed *THBS1-CD47* interaction only in the atherosclerotic condition, with the ligands originating in pericytes, SMCs, and ECs that signal to SMCs and lymphoid cells (Figure 5H). *THBS1*—thombospondin 1—is associated with vascular injury[52] and is known to induce fibrosis and inflammation and activate TGF-β signaling,[53,54] consistent with the atherosclerosis progression observed in our obese samples. Taken together, our data showcase alterations in cell communication in atherosclerosis and highlights central molecular networks involved in pathological atherogenesis and remodeling, including fibrosis, inflammation, and calcification.

Atherosclerosis signatures in the Ossabaw pig show a strong correlation to human disease

Given the importance of animal model systems to accurately recapitulate human disease states, we assessed the proximity of the Ossabaw pig model to human atherosclerosis and mouse atherosclerosis models (Figure 6A). We re-analyzed publicly available single-cell RNA sequencing (scRNA-seq) datasets of human atherosclerosis[37,55–57] and scRNA-seq datasets of mouse aortic disease and atherosclerosis.[37,58] Human datasets were integrated and clustered, and major cell types annotated (Figure S7A). Mouse datasets were analyzed separately due to differences in animal models, where mice only on high-fat diet (HFD) developed aortic disease,[58] while the *Apoe*$^{-/-}$ background and HFD were required for the development of atherosclerosis[37] (Figures S6B–S6C).

We initially identified human and mouse counterparts of cell populations detected in our pig dataset. Pig SMC_1 and SMC_2 displayed higher similarity to contractile SMCs in human and baseline SMCs in mouse, while SMC_3 and SMC_4 were most similar to transdifferentiating fibromyocytes, fibrochondrocytes, and FB subpopulations in human and mouse (Figures 6B and 6C). EC_1 and EC_4 were most similar to vasa vasorum ECs and inflammatory EC population in human, while EC_2 and EC_3 were associated with EndoMT transitioning ECs of intimal layer (Figure 6D). The number of immune and EC cell types was too low for similar analyses in mouse datasets. Pig immune cells also showed consistent similarity to human, with B cells being similar to plasma cells, B cells, and proliferating cells, while T cells were similar to two T cell populations and NK cells in human (Figure 6E). Myeloid-SMC-like cells were matched by SMC-like MFs in human atherosclerosis, while other MF subpopulations were most similar to human inflammatory and foamy MFs (Figure 6E).

We next compared gene expression changes in human and mouse atherosclerosis to the Ossabaw pig (Figures 6F and 6G). Only one human dataset, human coronary artery atherosclerosis,[55] had disease and control experimental groups that allowed for direct comparisons. Pig DEGs displayed moderate correlation with human coronary artery atherosclerosis, where SMCs and myeloid cells displayed the strongest similarity (Figure 6F). DEG analyses also revealed significant correlations between human and mouse (*Apoe*$^{-/-}$ model) in SMCs, ECs, and FBs (Figure 6G). Specifically, concordant changes of key atherosclerosis-associated genes such as *SPP1*, *APOE*, *IBSP*, *CD163*, and *TREM2* were observed[31,33] (Figure 6G). In contrast, gene expression changes in mouse aortic disease showed poor correlation to the pig aorta, emphasizing that HFD alone is insufficient to induce atherosclerosis in mice, while HF/HFru diet in Ossabaw pig can trigger disease without the need for further genetic modifications (Figure S8A). Moreover, we compared bulk RNA sequencing (RNA-seq) data from human abdominal aorta atherosclerotic lesions[59] with the Ossabaw pig aortas (Figure S8B). Pig DEGs in atherosclerosis correlated better with human abdominal aorta when compared with atherosclerosis samples from the coronary artery (Figure S8B), most likely due to the differences in the architecture and fluid dynamics of these vessels.

Together, our analyses reveal a positive correlation of pig data with human and mouse atherosclerosis, as well as presence of similar cellular transitions and upregulation of atherosclerosis-associated genes, emphasizing the suitability of Ossabaw pig model for preclinical CVD research.

DISCUSSION

In the current study, we characterized the Ossabaw pig model of atherosclerosis for further basic and preclinical studies via the single-cell transcriptomics approach. Our study revealed complex cellular adaptations and molecular interactions that occur in atherosclerosis in Ossabaw pig. We found involvement of the BDNF, TGF-β, and interleukin signaling pathways in atherosclerosis as a common mechanism affecting all vascular cell types. From single-cell profiles, we detected phenotypic switches in SMCs and immune cells, as well as EndoMT in intimal ECs. Furthermore, we characterized intercellular communication networks impeded by atherosclerosis, including pro-osteogenic *SPP1*, *PGE2*, and *SEMA3C* signaling. Through comparisons with atherosclerotic changes reported in mice and human, our work shows that the Ossabaw pig is a reliable model for atherosclerosis due to the similarity of molecular changes, as well as plaque characteristics such as naturally occurring calcification.

With the recent development of novel single-cell technologies, it has become possible to decipher tissue complexity and vascular heterogeneity on a previously unreachable level.[60–62] Several consortia took to create whole-organism single-cell atlases as a valuable scientific community resource.[63,64] Similarly, a pig atlas was recently developed.[65] It described multiple organs in great detail at baseline condition; however, CVD-relevant tissues such as aorta or carotid artery were not profiled. Sukhanov et al. utilized spatial transcriptomics platform to analyze plaques in the coronary artery of domesticated, familial hypercholesterolemic pigs.[66] An increase in the "fibromyocyte" population was reported in the plaque area, with upregulation of *THBS1*, *APOE*, *MMP9*, and *CTSD*, as well as AP-1-related genes, concordant with our findings. Here, we further deepen

(F and G) Correlation of DEGs between pig abdominal aorta atherosclerosis and (F) human coronary artery atherosclerosis scRNA-seq dataset[55] or (G) mouse ascending aorta atherosclerosis scRNA-seq.[37] Significant DEGs (p-adj $\leq$ 0.001, |log2FC| $\geq$ 1) from the pig dataset were utilized for these comparisons; R, Pearson's correlation coefficient.

the knowledge of pig atherosclerosis by providing the first high-resolution single-nucleus transcriptomic profile of healthy and atherosclerotic aortas in the Ossabaw pig, thus contributing to the publicly available single-cell resources.

Atherosclerotic plaques typically contain ECs, SMCs, and various inflammatory cells, including lipid-loaded foam cells.[67] We too detected these cell types, accompanied with other cell types originating in the adventitia (FBs, stromal, and Schwann cells). The SMCs in atherosclerosis significantly change their phenotype and undergo transdifferentiation. As such, "fibromyocyte"[37] or "fibrochondrocyte"[57] phenotypes have been reported in mouse and human atherosclerosis, as well as MF-like SMCs, characterized by expression of immune cell markers *CD45*, *CD68*, *LGALS3*, and *CD11b*, which contribute to the immune cell milieu of the plaque in mice.[34,68,69] Within atherosclerotic plaques analyzed here, SMCs presented a phenotypic switch to synthetic, pro-inflammatory, and pro-osteogenic fates that could be directly linked to human and mouse fibromyocyte and fibrochondrocyte subpopulations,[37,57] while MFs shifted toward an SMC-like phenotype (Figures 6B–6E). Pathways upregulated in Ossabaw pig atherosclerosis in ECs like EndoMT, TGF-β, and interleukin signaling were also consistent with human reports.[55] Similarly, atherosclerotic pig samples displayed stronger myeloid-SMC interactions (e.g., *SPP1* signaling [Figure 5]) in line with analyses on human plaques.[39,55]

Transcriptional changes observed in pig atherosclerosis showed a positive correlation with both human coronary and aortic atherosclerosis, as well as with mouse aortic atherosclerosis (Figures 6F and 6G). These findings collectively indicate that the Ossabaw pig model effectively mirrors features of human atherosclerosis development, supporting its suitability for CVD research. Of note, we showed that diet-induced aortic disease in wild-type mice had little to no correlation with the Ossabaw pig diet-induced atherosclerosis, and only genetically modified *Apoe*$^{-/-}$ mice could capture aspects of diet-induced atherosclerosis (Figures 6G and S8A). This emphasizes the simplicity of experimental design and the lack of genetic manipulations needed to induce atherosclerosis in the Ossabaw pig model.

Since the morphology of porcine atherosclerotic lesions is similar to that of human lesions, they are particularly fit for CVD research as an animal model. Their morphology, location within the vascular system, and developmental progress resemble the full complexity of lesions with necrotic cores, neovascularization, calcification, and thin fibrous caps in contrast to less complex mouse lesions.[7] Calcification of atherosclerotic plaques is frequently observed in humans. Therefore, the ability to naturally form calcium deposits in the plaque is of particular interest for the Ossabaw model. Calcification is associated with advanced plaque complexity, limiting acute and long-term outcomes after endovascular interventions.[70,71] Although several pathways promoting calcification have been identified, reasons underlying the higher susceptibility of certain arteries to calcification is still unclear.[72] We showed an upregulation of osteogenic markers such as *SPP1* and *IBSP*[31,33] and observed mild-to-severe aortic plaque calcification by histological stainings (Figures 1D, 1E, and S1D). The prevalence of calcification in human atherosclerosis ranges from 25% to 46% depending on the artery type and, in general, is more frequent in males compared to females.[70,71] It is positively correlated with increased body mass index and age and associated with vulnerable plaques and higher mortality rate.[70,71,73] While some of the mechanisms underlying the calcification process have been identified, the higher susceptibility of certain arteries still needs to be addressed.[72]

Vascular calcifications have also been reported in mouse models. The *Apoe*$^{-/-}$ mouse model displays vascular calcification at 12–18 months of age on a chow diet.[74] *Ldlr*$^{-/-}$ mice display calcification at 18 months on a chow diet and at 6 months on a Western diet, while mice injected with *Psck*9-AAV viruses display calcification at 12 months on a Western diet.[75] This implies that mouse models to study calcification are commonly attributed to senescent animals with relatively high disease burden. In case of Ossabaw pigs, we detected calcification of aortas at 25 months of age, equivalent to a mature adult but not yet senescent age.[76] Thus, due to physiological similarities of pig cardiovascular system to human and age-relevant calcification manifestation, the Ossabaw pig model of atherosclerosis provides an excellent opportunity to study mechanisms underlying calcification of plaques and its potential reversibility.

Limitations of the study

In the current study, we performed experiments on 5 castrated male pigs. While we recognize the limited sample number, our analyses nevertheless have sufficient statistical power to show the key features of atherosclerosis development including inflammation, phenotypic shifts of various cell types, and changes in cell communication. Unlike other studies, we could not observe cross-cell-type transitions (EC-immune and EC-SMC) in our dataset, which might be related to the conservative data preprocessing strategy. We removed doublets and nuclei with dual transcriptional identities (expressing several of major cell type markers) from the analysis, as we could not predict if those were real nuclei of "transitioning" cells or technical artifacts of the experimental method. We speculate that such transitioning cells may exist in the pig model similar to mouse or human; however, the confirmation will require further validation.

It is important to note genetic differences between pig breeds, as these genetic variations could also be responsible for differences in vascular function.[77,78] Ossabaw pigs possess a genetic predisposition for metabolic syndrome, display increased vasomotor reactivity to vasoconstricting agents and reduced vasodilation compared to Göttingen pigs, and are unresponsive to ischemic preconditioning.[77,78] These factors might play a role in the progression of atherosclerosis and results we observed. While studies have shown no difference in infarct size or treatment response between female and castrated male Ossabaw pigs,[78] it remains unclear if atherosclerosis formation in female Ossabaw pigs might display different dynamics compared to the castrated males used here. Estrogen manifests atheroprotective function in premenopausal females compared to males.[79,80] It might prevent atherosclerotic plaque formation during hormonal replacement therapy[81]; however, its effectiveness is still to be established.[82,83] More studies on female pigs will be necessary to determine the precise mechanisms underlying differences in phenotypes of CVD development and response to treatment in females.

Although the swine genome has been sequenced and annotated by Ensemble with high precision and accuracy,[17,84] a substantial proportion of pig genes have not been assigned their human orthologs or characterized. Despite conservation of major gene families between species, this knowledge gap can hinder some of the downstream analysis and interpretation of pig studies. In our study, we observed a high number of non-annotated genes downregulated across cell types in atherosclerosis (Figure S4B). We could still pursue GSEA and GO analyses to infer the downregulated pathways; however, the non-annotated genes could not be included in the analysis, which reduced its statistical power. Importantly, we also manually curated several novel gene annotations (Table S2), increasing the coverage of transcriptomic information.

In our single-cell analyses, we could only directly compare atherosclerosis-induced DEGs in Ossabaw pig aorta with human coronary artery atherosclerosis (Figure 6F) due to lack of human-derived single-cell datasets with healthy controls. Although the similarity between SMC, EC, and immune cell subtypes of swine aortic cells and human aortic, carotid, and coronary cells was high (Figures S7G–S7I), other vascular beds in human might provide better comparison with our pig model.

Lastly, we observed a discrepancy in immune cell representation of the plaques of our pig model compared to human atherosclerosis. Human atherosclerosis is characterized by increased T cell plaque infiltration and their gradual increase with disease progression.[43,85,86] On the other hand, the number of myeloid cells in human atherosclerosis is inversely correlated with age and complexity of the plaque.[87] While we detected both T cells and B cells in atherosclerosis in our pig model, the predominant immune cell type in the plaques was MFs and foamy cells, consistent with reports of mouse atherosclerosis models.[88,89] This discrepancy in human to pig to mouse is important to investigate, and it could be related to the atherosclerosis stage. Thus, further time-course studies of disease progression will be beneficial to test this hypothesis.

Taken together, we provide detailed insights into the Ossabaw pig model of atherosclerosis, thereby establishing a platform for preclinical screening of novel therapeutic interventions. Our transcriptomic analyses across species underpin the similarity of molecular and cellular mechanisms driving atherosclerosis development in human and the Ossabaw pig. Thus, utilization of the Ossabaw pig model will be an important tool to translate preclinical findings on cardiovascular health into human applications.

RESOURCE AVAILABILITY

Lead contact

Further information and requests for resources and reagents should be directed to and will be fulfilled by the lead contact, Olga Bondareva (olga.bondareva@helmholtz-munich.de).

Materials availability

This study did not generate new unique reagents.

Data and code availability

- Data: Original data produced in this work including raw sequencing data and Cell Ranger processed files can be found at GEO database, accession number GSE274218. Publicly available data used for inter-species analysis were downloaded from online repositories; see key resources table.
- Code: This study did not generate any novel analysis tools. The software used for analysis was downloaded online; see key resources table. Code used for the analysis and figure generation can be provided upon a request.
- All other items: N/A.

ACKNOWLEDGMENTS

We thank Minna Kaikkonen-Määttä and Terho Lehtimäki for helpful discussions. We are grateful to Daniela Kern for technical support and to Steffi Ines Anding, Janine Brunotte, Konstanze Julich-Gruner, Susanne Renno, and Sandra Zentile for administrative help. This work was financed by the HI-MAG institute budget of the program-oriented funding of the ENABLE program of the Helmholtz Association.

AUTHOR CONTRIBUTIONS

O.B., M.K., and S.S. conceptualized, initiated, and developed the project. P.M.H.H. provided the Ossabaw pigs and expertise in their handling. K.N. and S.O. took care of animal welfare. M.H., M.K., D.B., K.N., S.O., L.S., A.G., and S.S. undertook animal experiments and endovascular interventions. M.H. undertook histological analyses and quantification. O.B. developed the methodology for nuclei isolation, performed the single-nucleus transcriptomics experiments, and undertook bioinformatics analyses and curated the sequencing data. O.B., B.N.S., and S.S. supervised the project, provided guidance, and wrote the paper. S.S. acquired funding for the project. All authors read, edited, and approved the manuscript.

DECLARATION OF INTERESTS

S.S. serves as a consultant/advisory board member for Angiodynamics, Biotronik, Boston Scientific, Cook Medical, Medtronic, and Novartis. D.B. serves as an advisory board member for Medtronic and Terumo Aortic and received grants and speaking fees from Artivion, BD, Brainlab, Bentley Medical, Cook Medical, Getinge, and Endologix.

STAR★METHODS

Detailed methods are provided in the online version of this paper and include the following:

- KEY RESOURCES TABLE
- EXPERIMENTAL MODEL AND STUDY PARTICIPANT DETAILS
- METHOD DETAILS
  - Histochemical staining
  - ELISA assay
  - Preparation of single nuclei suspension and FACS
  - Single nuclei workflow
  - Bioinformatics analyses
- QUANTIFICATION AND STATISTICAL ANALYSIS

SUPPLEMENTAL INFORMATION

Supplemental information can be found online at https://doi.org/10.1016/j.isci.2025.113464.

Received: January 24, 2025
Revised: June 15, 2025
Accepted: August 26, 2025
Published: August 29, 2025

REFERENCES

1. World Health Organization (2020). Fact sheet - The top 10 causes of death. https://www.who.int/news-room/fact-sheets/detail/the-top-10-causes-of-death.

2. World Health Organization (2022). World health statistics 2022: monitoring health for the SDGs, sustainable development goals. https://www.who.int/publications/i/item/9789240051157.

3. Visseren, F.L.J., Mach, F., Smulders, Y.M., Carballo, D., Koskinas, K.C., Bäck, M., Benetos, A., Biffi, A., Boavida, J.M., Capodanno, D., et al. (2021). 2021 ESC Guidelines on cardiovascular disease prevention in clinical practice. Eur. Heart J. *42*, 3227–3337. https://doi.org/10.1093/eurheartj/ehab484.

4. Bellinger, D.A., Merricks, E.P., and Nichols, T.C. (2006). Swine models of type 2 diabetes mellitus: insulin resistance, glucose tolerance, and cardiovascular complications. ILAR J. *47*, 243–258. https://doi.org/10.1093/ilar.47.3.243.

5. Ludvigsen, T.P., Kirk, R.K., Christoffersen, B.Ø., Pedersen, H.D., Martinussen, T., Kildegaard, J., Heegaard, P.M.H., Lykkesfeldt, J., and Olsen, L.H. (2015). Göttingen minipig model of diet-induced atherosclerosis: influence of mild streptozotocin-induced diabetes on lesion severity and markers of inflammation evaluated in obese, obese and diabetic, and lean control animals. J. Transl. Med. *13*, 312. https://doi.org/10.1186/s12967-015-0670-2.

6. Swindle, M.M. (1998). Comparative anatomy and physiology of the pig. Scand. J. Lab. Anim. Sci. *25*, 11–21.

7. Sturek, M., Alloosh, M., and Sellke, F.W. (2020). Swine Disease Models for Optimal Vascular Engineering. Annu. Rev. Biomed. Eng. *22*, 25–49. https://doi.org/10.1146/annurev-bioeng-082919-053009.

8. Walters, E.M., and Prather, R.S. (2013). Advancing swine models for human health and diseases. Mo. Med. *110*, 212–215.

9. Gerrity, R.G., Natarajan, R., Nadler, J.L., and Kimsey, T. (2001). Diabetes-induced accelerated atherosclerosis in swine. Diabetes *50*, 1654–1665. https://doi.org/10.2337/diabetes.50.7.1654.

10. Ishii, A., Viñuela, F., Murayama, Y., Yuki, I., Nien, Y.L., Yeh, D.T., and Vinters, H.V. (2006). Swine model of carotid artery atherosclerosis: experimental induction by surgical partial ligation and dietary hypercholesterolemia. AJNR. Am. J. Neuroradiol. *27*, 1893–1899.

11. Sturek, M. (2011). Ca2+ regulatory mechanisms of exercise protection against coronary artery disease in metabolic syndrome and diabetes. J. Appl. Physiol. *111*, 573–586. https://doi.org/10.1152/japplphysiol.00373.2011.

12. Wilensky, R.L., Shi, Y., Mohler, E.R., 3rd, Hamamdzic, D., Burgert, M.E., Li, J., Postle, A., Fenning, R.S., Bollinger, J.G., Hoffman, B.E., et al. (2008). Inhibition of lipoprotein-associated phospholipase A2 reduces complex coronary atherosclerotic plaque development. Nat. Med. *14*, 1059–1066. https://doi.org/10.1038/nm.1870.

13. Edwards, J., Abdou, H., Patel, N., Madurska, M.J., Poe, K., Bonin, J.E., Richmond, M.J., Rasmussen, T.E., and Morrison, J.J. (2022). The functional vascular anatomy of the swine for research. Vascular *30*, 392–402. https://doi.org/10.1177/1708538121996500.

14. Hakansson, J., Simsa, R., Bogestal, Y., Jenndahl, L., Gustafsson-Hedberg, T., Petronis, S., Strehl, R., and Osterberg, K. (2021). Individualized tissue-engineered veins as vascular grafts: A proof of concept study in pig. J. Tissue Eng. Regen. Med. *15*, 818–830. https://doi.org/10.1002/term.3233.

15. Ishikawa, O., Tanaka, M., Konno, K., Hasebe, T., Horikawa, A., Iijima, A., Saito, N., and Takahashi, K. (2018). Swine model of in-stent stenosis in the iliac artery evaluating the serial time course. Exp. Anim. *67*, 501–508. https://doi.org/10.1538/expanim.18-0027.

16. Pedersen, R., Ingerslev, H.C., Sturek, M., Alloosh, M., Cirera, S., Christoffersen, B.Ø., Moesgaard, S.G., Larsen, N., and Boye, M. (2013). Characterisation of gut microbiota in Ossabaw and Gottingen minipigs as models of obesity and metabolic syndrome. PLoS One *8*, e56612. https://doi.org/10.1371/journal.pone.0056612.

17. Zhang, Y., Fan, G., Liu, X., Skovgaard, K., Sturek, M., and Heegaard, P.M.H. (2021). The genome of the naturally evolved obesity-prone Ossabaw miniature pig. iScience *24*, 103081. https://doi.org/10.1016/j.isci.2021.103081.

18. Badin, J.K., Kole, A., Stivers, B., Progar, V., Pareddy, A., Alloosh, M., and Sturek, M. (2018). Alloxan-induced diabetes exacerbates coronary atherosclerosis and calcification in Ossabaw miniature swine with metabolic syndrome. J. Transl. Med. *16*, 58. https://doi.org/10.1186/s12967-018-1431-9.

19. McKenney-Drake, M.L., Rodenbeck, S.D., Owen, M.K., Schultz, K.A., Alloosh, M., Tune, J.D., and Sturek, M. (2016). Repeat cross-sectional data on the progression of the metabolic syndrome in Ossabaw miniature swine. Data Brief *7*, 1393–1395. https://doi.org/10.1016/j.dib.2016.04.023.

20. McKenney, M.L., Schultz, K.A., Boyd, J.H., Byrd, J.P., Alloosh, M., Teague, S.D., Arce-Esquivel, A.A., Fain, J.N., Laughlin, M.H., Sacks, H.S., and Sturek, M. (2014). Epicardial adipose excision slows the progression of porcine coronary atherosclerosis. J. Cardiothorac. Surg. *9*, 2. https://doi.org/10.1186/1749-8090-9-2.

21. Yuan, F., Guo, L., Park, K.H., Woollard, J.R., Taek-Geun, K., Jiang, K., Melkamu, T., Zang, B., Smith, S.L., Fahrenkrug, S.C., et al. (2018). Ossabaw Pigs With a PCSK9 Gain-of-Function Mutation Develop Accelerated Coronary Atherosclerotic Lesions: A Novel Model for Preclinical Studies. J. Am. Heart Assoc. *7*, e006207. https://doi.org/10.1161/JAHA.117.006207.

22. Lafont, A. (2004). The Cypher stent: no longer efficacious at three months in the porcine model? Cardiovasc. Res. *63*, 575–576. https://doi.org/10.1016/j.cardiores.2004.06.016.

23. Virmani, R., Kolodgie, F.D., Burke, A.P., Farb, A., and Schwartz, S.M. (2000). Lessons from sudden coronary death: a comprehensive morphological classification scheme for atherosclerotic lesions. Arterioscler. Thromb. Vasc. Biol. *20*, 1262–1275. https://doi.org/10.1161/01.atv.20.5.1262.

24. Forcheron, F., Legedz, L., Chinetti, G., Feugier, P., Letexier, D., Bricca, G., and Beylot, M. (2005). Genes of cholesterol metabolism in human atheroma: overexpression of perilipin and genes promoting cholesterol storage and repression of ABCA1 expression. Arterioscler. Thromb. Vasc. Biol. *25*, 1711–1717. https://doi.org/10.1161/01.ATV.0000174123.19103.52.

25. Bondareva, O., Tsaryk, R., Bojovic, V., Odenthal-Schnittler, M., Siekmann, A.F., and Schnittler, H.J. (2019). Identification of atheroprone shear stress responsive regulatory elements in endothelial cells. Cardiovasc. Res. *115*, 1487–1499. https://doi.org/10.1093/cvr/cvz027.

26. Evrard, S.M., Lecce, L., Michelis, K.C., Nomura-Kitabayashi, A., Pandey, G., Purushothaman, K.R., d'Escamard, V., Li, J.R., Hadri, L., Fujitani, K., et al. (2016). Endothelial to mesenchymal transition is common in atherosclerotic lesions and is associated with plaque instability. Nat. Commun. *7*, 11853. https://doi.org/10.1038/ncomms11853.

27. Souilhol, C., Harmsen, M.C., Evans, P.C., and Krenning, G. (2018). Endothelial-mesenchymal transition in atherosclerosis. Cardiovasc. Res. *114*, 565–577. https://doi.org/10.1093/cvr/cvx253.

28. Tamargo, I.A., Baek, K.I., Kim, Y., Park, C., and Jo, H. (2023). Flow-induced reprogramming of endothelial cells in atherosclerosis. Nat. Rev. Cardiol. *20*, 738–753. https://doi.org/10.1038/s41569-023-00883-1.

29. Wang, K.C., Yeh, Y.T., Nguyen, P., Limqueco, E., Lopez, J., Thorossian, S., Guan, K.L., Li, Y.S.J., and Chien, S. (2016). Flow-dependent YAP/TAZ activities regulate endothelial phenotypes and atherosclerosis. Proc. Natl. Acad. Sci. USA *113*, 11525–11530. https://doi.org/10.1073/pnas.1613121113.

30. Zierold, S., Buschmann, K., Gachkar, S., Bochenek, M.L., Velmeden, D., Hobohm, L., Vahl, C.F., and Schäfer, K. (2021). Brain-Derived Neurotrophic Factor Expression and Signaling in Different Perivascular Adipose Tissue Depots of Patients With Coronary Artery Disease. J. Am. Heart Assoc. *10*, e018322. https://doi.org/10.1161/JAHA.120.018322.

31. Shanahan, C.M., Cary, N.R., Metcalfe, J.C., and Weissberg, P.L. (1994). High expression of genes for calcification-regulating proteins in human

atherosclerotic plaques. J. Clin. Investig. *93*, 2393–2402. https://doi.org/10.1172/JCI117246.

32. Speer, M.Y., Chien, Y.C., Quan, M., Yang, H.Y., Vali, H., McKee, M.D., and Giachelli, C.M. (2005). Smooth muscle cells deficient in osteopontin have enhanced susceptibility to calcification *in vitro*. Cardiovasc. Res. *66*, 324–333. https://doi.org/10.1016/j.cardiores.2005.01.023.
33. Dhore, C.R., Cleutjens, J.P., Lutgens, E., Cleutjens, K.B., Geusens, P.P., Kitslaar, P.J., Tordoir, J.H., Spronk, H.M., Vermeer, C., and Daemen, M. J. (2001). Differential expression of bone matrix regulatory proteins in human atherosclerotic plaques. Arterioscler. Thromb. Vasc. Biol. *21*, 1998–2003. https://doi.org/10.1161/hq1201.100229.
34. Shankman, L.S., Gomez, D., Cherepanova, O.A., Salmon, M., Alencar, G. F., Haskins, R.M., Swiatlowska, P., Newman, A.A.C., Greene, E.S., Straub, A.C., et al. (2015). KLF4-dependent phenotypic modulation of smooth muscle cells has a key role in atherosclerotic plaque pathogenesis. Nat. Med. *21*, 628–637. https://doi.org/10.1038/nm.3866.
35. Sun, Y., Byon, C.H., Yuan, K., Chen, J., Mao, X., Heath, J.M., Javed, A., Zhang, K., Anderson, P.G., and Chen, Y. (2012). Smooth muscle cell-specific runx2 deficiency inhibits vascular calcification. Circ. Res. *111*, 543–552. https://doi.org/10.1161/CIRCRESAHA.112.267237.
36. Cao, G., Xuan, X., Hu, J., Zhang, R., Jin, H., and Dong, H. (2022). How vascular smooth muscle cell phenotype switching contributes to vascular disease. Cell Commun. Signal. *20*, 180. https://doi.org/10.1186/s12964-022-00993-2.
37. Wirka, R.C., Wagh, D., Paik, D.T., Pjanic, M., Nguyen, T., Miller, C.L., Kundu, R., Nagao, M., Coller, J., Koyano, T.K., et al. (2019). Atheroprotective roles of smooth muscle cell phenotypic modulation and the TCF21 disease gene as revealed by single-cell analysis. Nat. Med. *25*, 1280–1289. https://doi.org/10.1038/s41591-019-0512-5.
38. Zhou, M., Zhu, Y., Zhou, Z., Qi, F., Zheng, S., Gao, S., Li, Y., Liu, Y., and Du, J. (2022). Fibroblast-Secreted Phosphoprotein 1 Mediates Extracellular Matrix Deposition and Inhibits Smooth Muscle Cell Contractility in Marfan Syndrome Aortic Aneurysm. J. Cardiovasc. Transl. Res. *15*, 959–970. https://doi.org/10.1007/s12265-022-10239-8.
39. Mosquera, J.V., Auguste, G., Wong, D., Turner, A.W., Hodonsky, C.J., Alvarez-Yela, A.C., Song, Y., Cheng, Q., Lino Cardenas, C.L., Theofilatos, K., et al. (2023). Integrative single-cell meta-analysis reveals disease-relevant vascular cell states and markers in human atherosclerosis. Cell Rep. *42*, 113380. https://doi.org/10.1016/j.celrep.2023.113380.
40. Trimm, E., and Red-Horse, K. (2023). Vascular endothelial cell development and diversity. Nat. Rev. Cardiol. *20*, 197–210. https://doi.org/10.1038/s41569-022-00770-1.
41. Vanlandewijck, M., He, L., Mäe, M.A., Andrae, J., Ando, K., Del Gaudio, F., Nahar, K., Lebouvier, T., Laviña, B., Gouveia, L., et al. (2018). A molecular atlas of cell types and zonation in the brain vasculature. Nature *554*, 475–480. https://doi.org/10.1038/nature25739.
42. Simons, M., Gordon, E., and Claesson-Welsh, L. (2016). Mechanisms and regulation of endothelial VEGF receptor signalling. Nat. Rev. Mol. Cell Biol. *17*, 611–625. https://doi.org/10.1038/nrm.2016.87.
43. Depuydt, M.A.C., Prange, K.H.M., Slenders, L., Örd, T., Elbersen, D., Boltjes, A., de Jager, S.C.A., Asselbergs, F.W., de Borst, G.J., Aavik, E., et al. (2020). Microanatomy of the Human Atherosclerotic Plaque by Single-Cell Transcriptomics. Circ. Res. *127*, 1437–1455. https://doi.org/10.1161/CIRCRESAHA.120.316770.
44. Cochain, C., Vafadarnejad, E., Arampatzi, P., Pelisek, J., Winkels, H., Ley, K., Wolf, D., Saliba, A.E., and Zernecke, A. (2018). Single-Cell RNA-Seq Reveals the Transcriptional Landscape and Heterogeneity of Aortic Macrophages in Murine Atherosclerosis. Circ. Res. *122*, 1661–1674. https://doi.org/10.1161/CIRCRESAHA.117.312509.
45. Zernecke, A., Winkels, H., Cochain, C., Williams, J.W., Wolf, D., Soehnlein, O., Robbins, C.S., Monaco, C., Park, I., McNamara, C.A., et al. (2020). Meta-Analysis of Leukocyte Diversity in Atherosclerotic Mouse Aortas. Circ. Res. *127*, 402–426. https://doi.org/10.1161/CIRCRESAHA.120.316903.
46. Jin, S., Plikus, M.V., and Nie, Q. (2023). CellChat for systematic analysis of cell-cell communication from single-cell and spatially resolved transcriptomics. Preprint at bioRxiv. https://doi.org/10.1101/2023.11.05.565674.
47. Kaji, H., Sugimoto, T., Kanatani, M., Fukase, M., Kumegawa, M., and Chihara, K. (1996). Prostaglandin E2 stimulates osteoclast-like cell formation and bone-resorbing activity via osteoblasts: role of cAMP-dependent protein kinase. J. Bone Miner. Res. *11*, 62–71. https://doi.org/10.1002/jbmr.5650110110.
48. Kobayashi, Y., Mizoguchi, T., Take, I., Kurihara, S., Udagawa, N., and Takahashi, N. (2005). Prostaglandin E2 enhances osteoclastic differentiation of precursor cells through protein kinase A-dependent phosphorylation of TAK1. J. Biol. Chem. *280*, 11395–11403. https://doi.org/10.1074/jbc.M411189200.
49. Nam, J.S., Ahn, C.W., Park, H.J., and Kim, Y.S. (2020). Semaphorin 3 C is a Novel Adipokine Representing Exercise-Induced Improvements of Metabolism in Metabolically Healthy Obese Young Males. Sci. Rep. *10*, 10005. https://doi.org/10.1038/s41598-020-67004-7.
50. Mejhert, N., Wilfling, F., Esteve, D., Galitzky, J., Pellegrinelli, V., Kolditz, C. I., Viguerie, N., Tordjman, J., Näslund, E., Trayhurn, P., et al. (2013). Semaphorin 3C is a novel adipokine linked to extracellular matrix composition. Diabetologia *56*, 1792–1801. https://doi.org/10.1007/s00125-013-2931-z.
51. Toma, I., and McCaffrey, T.A. (2012). Transforming growth factor-beta and atherosclerosis: interwoven atherogenic and atheroprotective aspects. Cell Tissue Res. *347*, 155–175. https://doi.org/10.1007/s00441-011-1189-3.
52. Moura, R., Tjwa, M., Vandervoort, P., Cludts, K., and Hoylaerts, M.F. (2007). Thrombospondin-1 activates medial smooth muscle cells and triggers neointima formation upon mouse carotid artery ligation. Arterioscler. Thromb. Vasc. Biol. *27*, 2163–2169. https://doi.org/10.1161/ATVBAHA.107.151282.
53. Kumar, R., Mickael, C., Kassa, B., Gebreab, L., Robinson, J.C., Koyanagi, D.E., Sanders, L., Barthel, L., Meadows, C., Fox, D., et al. (2017). TGF-beta activation by bone marrow-derived thrombospondin-1 causes Schistosoma- and hypoxia-induced pulmonary hypertension. Nat. Commun. *8*, 15494. https://doi.org/10.1038/ncomms15494.
54. Raman, P., Krukovets, I., Marinic, T.E., Bornstein, P., and Stenina, O.I. (2007). Glycosylation mediates up-regulation of a potent antiangiogenic and proatherogenic protein, thrombospondin-1, by glucose in vascular smooth muscle cells. J. Biol. Chem. *282*, 5704–5714. https://doi.org/10.1074/jbc.M610965200.
55. Alsaigh, T., Evans, D., Frankel, D., and Torkamani, A. (2022). Decoding the transcriptome of calcified atherosclerotic plaque at single-cell resolution. Commun. Biol. *5*, 1084. https://doi.org/10.1038/s42003-022-04056-7.
56. Hu, Z., Liu, W., Hua, X., Chen, X., Chang, Y., Hu, Y., Xu, Z., and Song, J. (2021). Single-Cell Transcriptomic Atlas of Different Human Cardiac Arteries Identifies Cell Types Associated With Vascular Physiology. Arterioscler. Thromb. Vasc. Biol. *41*, 1408–1427. https://doi.org/10.1161/ATVBAHA.120.315373.
57. Pan, H., Xue, C., Auerbach, B.J., Fan, J., Bashore, A.C., Cui, J., Yang, D. Y., Trignano, S.B., Liu, W., Shi, J., et al. (2020). Single-Cell Genomics Reveals a Novel Cell State During Smooth Muscle Cell Phenotypic Switching and Potential Therapeutic Targets for Atherosclerosis in Mouse and Human. Circulation *142*, 2060–2075. https://doi.org/10.1161/CIRCULATIONAHA.120.048378.
58. Kan, H., Zhang, K., Mao, A., Geng, L., Gao, M., Feng, L., You, Q., and Ma, X. (2021). Single-cell transcriptome analysis reveals cellular heterogeneity in the ascending aortas of normal and high-fat diet-fed mice. Exp. Mol. Med. *53*, 1379–1389. https://doi.org/10.1038/s12276-021-00671-2.
59. Sulkava, M., Raitoharju, E., Levula, M., Seppälä, I., Lyytikäinen, L.P., Mennander, A., Järvinen, O., Zeitlin, R., Salenius, J.P., Illig, T., et al. (2017). Differentially expressed genes and canonical pathway expression in human atherosclerotic plaques - Tampere Vascular Study. Sci. Rep. *7*, 41483. https://doi.org/10.1038/srep41483.

60. Kalucka, J., de Rooij, L.P.M.H., Goveia, J., Rohlenova, K., Dumas, S.J., Meta, E., Conchinha, N.V., Taverna, F., Teuwen, L.A., Veys, K., et al. (2020). Single-Cell Transcriptome Atlas of Murine Endothelial Cells. Cell *180*, 764–779.e20. https://doi.org/10.1016/j.cell.2020.01.015.

61. Bondareva, O., Rodríguez-Aguilera, J.R., Oliveira, F., Liao, L., Rose, A., Gupta, A., Singh, K., Geier, F., Schuster, J., Boeckel, J.N., et al. (2022). Single-cell profiling of vascular endothelial cells reveals progressive organ-specific vulnerabilities during obesity. Nat. Metab. *4*, 1591–1610. https://doi.org/10.1038/s42255-022-00674-x.

62. Bondareva, O., and Sheikh, B.N. (2020). Vascular Homeostasis and Inflammation in Health and Disease-Lessons from Single Cell Technologies. Int. J. Mol. Sci. *21*, 4688. https://doi.org/10.3390/ijms21134688.

63. Rozenblatt-Rosen, O., Stubbington, M.J.T., Regev, A., and Teichmann, S. A. (2017). The Human Cell Atlas: from vision to reality. Nature *550*, 451–453. https://doi.org/10.1038/550451a.

64. Tabula Muris Consortium; Overall coordination; Logistical coordination; Organ collection and processing; Library preparation and sequencing; Writing group; Supplemental text writing group; Principal investigatorsse-quencing; Computational data analysis; Cell type annotation (2018). Single-cell transcriptomics of 20 mouse organs creates a Tabula Muris. Nature *562*, 367–372. https://doi.org/10.1038/s41586-018-0590-4.

65. Wang, F., Ding, P., Liang, X., Ding, X., Brandt, C.B., Sjöstedt, E., Zhu, J., Bolund, S., Zhang, L., de Rooij, L.P.M.H., et al. (2022). Endothelial cell heterogeneity and microglia regulons revealed by a pig cell landscape at single-cell level. Nat. Commun. *13*, 3620. https://doi.org/10.1038/s41467-022-31388-z.

66. Sukhanov, S., Higashi, Y., Yoshida, T., Danchuk, S., Alfortish, M., Goodchild, T., Scarborough, A., Sharp, T., Jenkins, J.S., Garcia, D., et al. (2023). Insulin-like growth factor 1 reduces coronary atherosclerosis in pigs with familial hypercholesterolemia. JCI Insight *8*, e165713. https://doi.org/10.1172/jci.insight.165713.

67. Wolf, D., and Ley, K. (2019). Immunity and Inflammation in Atherosclerosis. Circ. Res. *124*, 315–327. https://doi.org/10.1161/CIRCRESAHA.118.313591.

68. Feil, S., Fehrenbacher, B., Lukowski, R., Essmann, F., Schulze-Osthoff, K., Schaller, M., and Feil, R. (2014). Transdifferentiation of vascular smooth muscle cells to macrophage-like cells during atherogenesis. Circ. Res. *115*, 662–667. https://doi.org/10.1161/CIRCRESAHA.115.304634.

69. Li, Y., Zhu, H., Zhang, Q., Han, X., Zhang, Z., Shen, L., Wang, L., Lui, K.O., He, B., and Zhou, B. (2021). Smooth muscle-derived macrophage-like cells contribute to multiple cell lineages in the atherosclerotic plaque. Cell Discov. *7*, 111. https://doi.org/10.1038/s41421-021-00328-4.

70. Kamenskiy, A., Poulson, W., Sim, S., Reilly, A., Luo, J., and MacTaggart, J. (2018). Prevalence of Calcification in Human Femoropopliteal Arteries and its Association with Demographics, Risk Factors, and Arterial Stiffness. Arterioscler. Thromb. Vasc. Biol. *38*, e48–e57. https://doi.org/10.1161/ATVBAHA.117.310490.

71. Chen, S., Li, N., Gao, Y., Jiang, H., and Shen, Y. (2022). Prevalence and risk factors for vascular calcification based on the ankle-brachial index in the general population: a cross-sectional study. BMC Cardiovasc. Disord. *22*, 227. https://doi.org/10.1186/s12872-022-02668-9.

72. Demer, L.L., and Tintut, Y. (2008). Vascular calcification: pathobiology of a multifaceted disease. Circulation *117*, 2938–2948. https://doi.org/10.1161/CIRCULATIONAHA.107.743161.

73. Alexopoulos, N., and Raggi, P. (2009). Calcification in atherosclerosis. Nat. Rev. Cardiol. *6*, 681–688. https://doi.org/10.1038/nrcardio.2009.165.

74. Rattazzi, M., Bennett, B.J., Bea, F., Kirk, E.A., Ricks, J.L., Speer, M., Schwartz, S.M., Giachelli, C.M., and Rosenfeld, M.E. (2005). Calcification of advanced atherosclerotic lesions in the innominate arteries of ApoE-deficient mice: potential role of chondrocyte-like cells. Arterioscler. Thromb. Vasc. Biol. *25*, 1420–1425. https://doi.org/10.1161/01.ATV.0000166600.58468.1b.

75. Awan, Z., Denis, M., Bailey, D., Giaid, A., Prat, A., Goltzman, D., Seidah, N. G., and Genest, J. (2011). The LDLR deficient mouse as a model for aortic calcification and quantification by micro-computed tomography. Atherosclerosis *219*, 455–462. https://doi.org/10.1016/j.atherosclerosis.2011.08.035.

76. Tohyama, S., and Kobayashi, E. (2019). Age-Appropriateness of Porcine Models Used for Cell Transplantation. Cell Transplant. *28*, 224–228. https://doi.org/10.1177/0963689718817477.

77. Eickelmann, C., Lieder, H.R., Sturek, M., Heusch, G., and Kleinbongard, P. (2024). Differences in vasomotor function of mesenteric arteries between Ossabaw minipigs with predisposition to metabolic syndrome and Gottingen minipigs. Am. J. Physiol. Heart Circ. Physiol. *326*, H408–H417. https://doi.org/10.1152/ajpheart.00719.2023.

78. Kleinbongard, P., Lieder, H.R., Skyschally, A., Alloosh, M., Gödecke, A., Rahmann, S., Sturek, M., and Heusch, G. (2022). Non-responsiveness to cardioprotection by ischaemic preconditioning in Ossabaw minipigs with genetic predisposition to, but without the phenotype of the metabolic syndrome. Basic Res. Cardiol. *117*, 58. https://doi.org/10.1007/s00395-022-00965-0.

79. Adams, M.R., Williams, J.K., and Kaplan, J.R. (1995). Effects of androgens on coronary artery atherosclerosis and atherosclerosis-related impairment of vascular responsiveness. Arterioscler. Thromb. Vasc. Biol. *15*, 562–570. https://doi.org/10.1161/01.atv.15.5.562.

80. Hakamaa, E., Goebeler, S., Martiskainen, M., Louhelainen, A.M., Ahinko, K., Lehtimäki, T., and Karhunen, P. (2024). Sex differences in coronary atherosclerosis during the pre- and postmenopausal period: The Tampere Sudden Death Study. Atherosclerosis *390*, 117459. https://doi.org/10.1016/j.atherosclerosis.2024.117459.

81. Hodis, H.N., Mack, W.J., Lobo, R.A., Shoupe, D., Sevanian, A., Mahrer, P. R., Selzer, R.H., Liu Cr, C.R., Liu Ch, C.H., and Azen, S.P.; Estrogen in the Prevention of Atherosclerosis Trial Research Group (2001). Estrogen in the prevention of atherosclerosis. A randomized, double-blind, placebo-controlled trial. Ann. Intern. Med. *135*, 939–953. https://doi.org/10.7326/0003-4819-135-11-200112040-00005.

82. Kakibuchi, A., Ito, F., Takaoka, O., Tahara, N., Kawamata, M., Yabumoto, K., Katayama, A., Izumi, Y., Maeda, E., and Mori, T. (2025). Effects of 17beta-estradiol and equilin on atherosclerosis development in female Apoe(shl) mice. Sci. Rep. *15*, 24922. https://doi.org/10.1038/s41598-025-10494-0.

83. Xu, T., Cai, J., Wang, L., Xu, L., Zhao, H., Wang, F., Meyron-Holtz, E.G., Missirlis, F., Qiao, T., and Li, K. (2023). Hormone replacement therapy for postmenopausal atherosclerosis is offset by late age iron deposition. eLife *12*, e80494. https://doi.org/10.7554/eLife.80494.

84. Martin, F.J., Amode, M.R., Aneja, A., Austine-Orimoloye, O., Azov, A.G., Barnes, I., Becker, A., Bennett, R., Berry, A., Bhai, J., et al. (2023). Ensembl 2023. Nucleic Acids Res. *51*, D933–D941. https://doi.org/10.1093/nar/gkac958.

85. Fernandez, D.M., Rahman, A.H., Fernandez, N.F., Chudnovskiy, A., Amir, E.A.D., Amadori, L., Khan, N.S., Wong, C.K., Shamailova, R., Hill, C.A., et al. (2019). Single-cell immune landscape of human atherosclerotic plaques. Nat. Med. *25*, 1576–1588. https://doi.org/10.1038/s41591-019-0590-4.

86. van Dijk, R.A., Duinisveld, A.J.F., Schaapherder, A.F., Mulder-Stapel, A., Hamming, J.F., Kuiper, J., de Boer, O.J., van der Wal, A.C., Kolodgie, F. D., Virmani, R., and Lindeman, J.H.N. (2015). A change in inflammatory footprint precedes plaque instability: a systematic evaluation of cellular aspects of the adaptive immune response in human atherosclerosis. J. Am. Heart Assoc. *4*, e001403. https://doi.org/10.1161/JAHA.114.001403.

87. van Dijk, R.A., Virmani, R., von der Thüsen, J.H., Schaapherder, A.F., and Lindeman, J.H.N. (2010). The natural history of aortic atherosclerosis: a systematic histopathological evaluation of the peri-renal region. Atherosclerosis *210*, 100–106. https://doi.org/10.1016/j.atherosclerosis.2009.11.016.

88. Zernecke, A., Erhard, F., Weinberger, T., Schulz, C., Ley, K., Saliba, A.E., and Cochain, C. (2023). Integrated single-cell analysis-based classification of vascular mononuclear phagocytes in mouse and human atherosclerosis. Cardiovasc. Res. *119*, 1676–1689. https://doi.org/10.1093/cvr/cvac161.

89. Winkels, H., Ehinger, E., Vassallo, M., Buscher, K., Dinh, H.Q., Kobiyama, K., Hamers, A.A.J., Cochain, C., Vafadarnejad, E., Saliba, A.E., et al. (2018). Atlas of the Immune Cell Repertoire in Mouse Atherosclerosis Defined by Single-Cell RNA-Sequencing and Mass Cytometry. Circ. Res. *122*, 1675–1688. https://doi.org/10.1161/CIRCRESAHA.117.312513.

90. Nothjunge, S., Nührenberg, T.G., Grüning, B.A., Doppler, S.A., Preissl, S., Schwaderer, M., Rommel, C., Krane, M., Hein, L., and Gilsbach, R. (2017). DNA methylation signatures follow preformed chromatin compartments in cardiac myocytes. Nat. Commun. *8*, 1667. https://doi.org/10.1038/s41467-017-01724-9.

91. Satija, R., Farrell, J.A., Gennert, D., Schier, A.F., and Regev, A. (2015). Spatial reconstruction of single-cell gene expression data. Nat. Biotechnol. *33*, 495–502. https://doi.org/10.1038/nbt.3192.

92. Young, M.D., and Behjati, S. (2020). SoupX removes ambient RNA contamination from droplet-based single-cell RNA sequencing data. GigaScience *9*, giaa151. https://doi.org/10.1093/gigascience/giaa151.

93. McGinnis, C.S., Murrow, L.M., and Gartner, Z.J. (2019). DoubletFinder: Doublet Detection in Single-Cell RNA Sequencing Data Using Artificial Nearest Neighbors. Cell Syst. *8*, 329–337.e4. https://doi.org/10.1016/j.cels.2019.03.003.

94. Korsunsky, I., Millard, N., Fan, J., Slowikowski, K., Zhang, F., Wei, K., Baglaenko, Y., Brenner, M., Loh, P.R., and Raychaudhuri, S. (2019). Fast, sensitive and accurate integration of single-cell data with Harmony. Nat. Methods *16*, 1289–1296. https://doi.org/10.1038/s41592-019-0619-0.

95. Ianevski, A., Giri, A.K., and Aittokallio, T. (2022). Fully-automated and ultra-fast cell-type identification using specific marker combinations from single-cell transcriptomic data. Nat. Commun. *13*, 1246. https://doi.org/10.1038/s41467-022-28803-w.

96. Yu, G., Wang, L.G., Han, Y., and He, Q.Y. (2012). clusterProfiler: an R package for comparing biological themes among gene clusters. OMICS *16*, 284–287. https://doi.org/10.1089/omi.2011.0118.

97. Xie, Z., Bailey, A., Kuleshov, M.V., Clarke, D.J.B., Evangelista, J.E., Jenkins, S.L., Lachmann, A., Wojciechowicz, M.L., Kropiwnicki, E., Jagodnik, K.M., et al. (2021). Gene Set Knowledge Discovery with Enrichr. Curr. Protoc. *1*, e90. https://doi.org/10.1002/cpz1.90.

98. González-Velasco, Ó., Sanchez-Luis, E., De La Rosa, E., Sánchez-Santos, J.M., and De Las Rivas, J. (2022). A single-cell clusters similarity measure for different batches, datasets, and samples. Preprint at bioRxiv. https://doi.org/10.1101/2022.03.14.483731.

STAR★METHODS

KEY RESOURCES TABLE

REAGENT or RESOURCE	SOURCE	IDENTIFIER
Antibodies		
Monoclonal mouse anti-CD68	DAKO	M0876; RRID: AB_2074844
Chemicals, peptides, and recombinant proteins		
5% silver nitrate		
Oil Red O staining		
Nuclear fast red-aluminum sulfate solution	Carl Roth	N069.1
Critical commercial assays		
Movat Pentachrome Stain Kit, Modified Russell-Movat	SkyTec laboratories	Inc. MPS-1
ROTI® Histokit	Carl Roth	6638.1
EnVision+System-HRP	DAKO	K4003
ELISA HDL/LDL cholesterol	CliniSciences	MBS168251-192
10x Next GEM Single Cell 3 GEM kit v3.1	10x Genomics	PN-1000121
Deposited data		
Raw & processed snRNA sequencing data	This paper	GEO: GSE274218
Sscrofa11.1 reference pig genome	Ensembl	https://www.ensembl.org/Sus_scrofa/Info/Annotation
Human coronary artery atherosclerosis	Wirka et al.[37]	GEO: GSE131778
Mouse ascending aorta atherosclerosis	Wirka et al.[37]	GEO: GSE131776
Human coronary artery atherosclerosis	Alsaigh et al.[55]	GEO: GSE159677
Human cardiac arteries	Hu et al.[56]	https://doi.org/10.1161/ATVBAHA.120.315373
Human atherosclerotic carotid arteries	Pan et al.[57]	GEO: GSE155512
Mouse aortic disease	Kan et al.[58]	https://doi.org/10.1038/s12276-021-00671-2
Bulk RNA-seq data from human abdominal aorta atherosclerotic lesions	Sulkava et al.[59]	https://doi.org/10.1038/srep41483
Experimental models: Organisms/strains		
Ossabaw pigs	Ossabaw breeding facility at the TU of Denmark (DTU)	https://ossabaw.dtu.dk
Software and algorithms		
Cell Ranger v5.0.1	10x Genomics	https://www.10xgenomics.com/support/software/cell-ranger/latest
Seurat package v5.0	Satija et al.[4]	https://satijalab.org/seurat/
SoupX	Young et al.[5]	https://github.com/constantAmateur/SoupX
DoubletFinder	McGinnis et al.[6]	https://github.com/chris-mcginnis-ucsf/DoubletFinder
Harmony	Korsunsky et al.[7]	https://github.com/immunogenomics/harmony
ScType	Ianevski et al.[11]	https://github.com/IanevskiAleksandr/sc-type
ClusterProfiler	Yu et al.[13]	https://guangchuangyu.github.io/software/clusterProfiler/
Enrichr	Xie et al.[14]	https://maayanlab.cloud/Enrichr/
CellChat	Jin et al.[15]	https://github.com/sqjin/CellChat

(*Continued on next page*)

Continued

REAGENT or RESOURCE	SOURCE	IDENTIFIER
ClusterFoldSimilarity	González-Velasco et al.[21]	https://github.com/OscarGVelasco/ClusterFoldSimilarity
Other		
High fat/ high fructose (HF/HFru), 2% cholesterol diet	- CorVus Biomedical LLC - Ssniff Spezialdiäten GmbH	- KT324 - S0602-S300S
Chow diet	Special Diets Services	Mini-pig diet SMP(E) 801586
gentleMACS C-tubes	Milteny Biotec	130-096-334
gentleMACS^{TM} Octo Dissociator	Milteny Biotec	–

EXPERIMENTAL MODEL AND STUDY PARTICIPANT DETAILS

All experiments were performed in accordance with the German Animal Welfare Law, and were approved by the state animal ethics committee, registration number: 25-5131/51/21 (Landesdirektion Sachsen, Leipzig, Germany). Ossabaw pigs (N = 4 and 3 pigs in obese and control groups, respectively) were obtained from the Ossabaw facility at the Technical University of Denmark (DTU) (https://ossabaw.dtu.dk). Animals were kept at natural light cycle (light/dark cycle of 12:12 with dawn) with a temperature of 20 ± 2°C and allowed *ad libitum* access to water. They were given straw bedding or wood shaving on rubber mat and had constant access to enrichment. The obesogenic feeding procedure and all other procedures used were approved by the Danish Animal Experiments Inspectorate (permit 2016-15-0201-01022), complied with the ARRIVE guidelines and were done in accordance with Danish laws and regulations regarding the use of animals in research (The Danish Ministry of Justice, Act on Animal Experiments no. 474 of 15 May 2014, as stipulated in the executive order no. 12 on 7 January 2016) and by the state animal ethics committee (Landesdirektion Sachsen, Leipzig, Germany). Starting at 16 months of age castrated male Ossabaw pigs were put either on a high-caloric high fat/high fructose (HF/HFru), 2% cholesterol diet (CorVus Biomedical LLC, KT324; Ssniff Spezialdiäten GmbH, S0602-S300S) or control chow diet (Special Diets Services; Mini-pig diet SMP(E) 801586). The HF/HFru diet consists of 16.3% kcal protein, 40.8% kcal carbohydrates (including 19% kcal from fructose), and 42.9% kcal fat, and is specifically designed for Ossabaw pigs for development of metabolic syndrome and hypercholesterolenemia.[18,19] All Ossabaw pigs were housed at the Ossabaw facility at the Technical University of Denmark (DTU) for the control and partially for the obesity feeding period (6 months), followed by transport and obesity feeding period (additional 3 months) in Leipzig, Germany. Prior to termination, animals were anesthetized. Vessel dissection was performed by certified surgeons. The samples were taken from abdominal aortic regions between renal and iliac arteries branching points, and either fixed in formalin solution overnight at 4°C, or directly snap-frozen in liquid nitrogen and stored at -80°C. Samples from 1 control sample could not be retrieved.

METHOD DETAILS

Histochemical staining

Aorta sections were cut into approximately 1 cm^3 pieces and fixed with PBS-buffered formalin solution overnight at 4°C. Tissues were embedded in paraffin and 5 μm sections cut using a microtome (Thermo Scientific HM355S) and attached to Superfrost slides (Epredia J1800AMNZ). Two segments of the aorta were prepared from each animal (descending aorta, iliac aorta). Three areas from each segment were observed at 250 μm intervals. The sections were de-paraffinized and hydrated. Tissue area was outlined with a Pap Pen (Kisker MKP-2).

Movat Pentachrome staining was performed with the Movat Pentachrome Stain Kit, Modified Russell-Movat (SkyTec laboratories, Inc. MPS-1). The incubation times were adjusted to the tissue. In addition, to stain and differentiate the elastic fibers (black), the staining solution was mounted for 25 min on slides, followed by 2% ferric chloride solution mount 3 x 1 min. The differentiation of the muscle fibers (red) was modified in the same way. To reduce yellow background slides were immersed in 80% ethanol prior to dehydrating and final covering in ROTI® Histokit (Carl Roth 6638.1).

Von Kossa silver staining was performed on de-paraffinized and hydrated sections. Briefly, slides were incubated for 30 min in 5% silver nitrate, washed, and incubated for 2 min in 5% sodium carbonate in 10% formalin solution. Sections then were washed, fixed in 5% sodium thiosulphate, counterstained with nuclear fast red-aluminum sulfate solution (Carl Roth N069.1) for 3 min, and covered with ROTI® Histokit (Carl Roth 6638.1).

Oil Red O staining was performed on frozen slides equilibrated in 60% isopropanol. Oil Red O working solution (3V: 2V distilled H2O) was incubated for 15 min at RT, briefly incubated in 60% isopropanol, washed in distilled H2O, and counted stained with nuclei staining with Hamatoxilin.

CD68 staining was performed on deparaffinized slides after the antigen retrieval. The slides were blocked for 30 min in 10% Methanol + 3% H2O2 in distilled H2O, and stained overnight in 1:100 CD68 antibody (DAKO, M0876). Next day the staining was developed with DAKO EnVision+System-HRP for 30 min followed by nuclei staining with Hamatoxilin.

Slides were visualized using fluorescent microscope Keyence BZ-X810. The same image exposure and acquisition settings were used for all sections. Three slides per segment of aorta, two segments per animal (N = 4 and 2 pigs in obese and control groups, respectively) were acquired. Quantification was done using the Keyence software by manually measuring intima and media thickness at the largest distance between 2 points in 3 individual ROI per image, and by ImageJ software, WandAutoMeasureTool for measuring stenosis grade. Then, the data were averaged per image, and the non-parametric Mann-Whitney test was performed (GraphPad Prism 10).

ELISA assay

ELISA assay measuring HDL/LDL cholesterol levels (CliniSciences, # MBS168251-192) was performed on animal's serum isolated before start of obesogenic diet and at the end of the treatment according to the manufacturer's protocol.

Preparation of single nuclei suspension and FACS

To preserve true tissue composition proportions and avoid damage of more sensitive cells, we opted for single nuclei RNA-seq. Snap frozen aortic tissue was stored at -80°C until nuclei isolation took place. To mitigate the possible batch effects of sample handling, all samples were processed simultaneously. FACS isolation of nuclei was undertaken as previously described with several modifications.[90] For each sample, a piece of frozen vessel tissue approximately 50 mm length was cut on dry ice to avoid thawing, and transferred directly into a gentleMACS C-tube (Milteny Biotec 130-096-334) containing nuclei isolation buffer (NIB) (5 mM CaCl2; 3mM MgAc; 2 mM EDTA; 0.5 mM EGTA; 10 mM Tris-HCl, pH 8; cOmplete protease inhibitor cocktail, Roche; 1 mM dithiothreitol; RNAse OUT™ , Invitrogen). It was further dissociated with the gentleMACS™ Octo Dissociator system with heaters using the "protein_01" protocol at 4°C. The nuclei suspension was rinsed with NIB supplemented with 0.4% Triton X-100 to final 0.2% concentration, filtered through a 70 μm cell strainer and the cell strainer was rinsed once with 10 ml FACS buffer (2% FCS in PBS (Sigma D8537)). Nuclei were collected via centrifugation (4°C, 1000 g, for 5 min), resuspended in FACS buffer and passed through a 40 μm cell strainer into a FACS tube. All samples were stained with the DRAQ5 stain (1:100, Cell Signaling Technology) diluted in FACS buffer for 10 min on ice in a total volume of 1 ml. Intact single nuclei were sorted on the FACS Melody (BD Biosciences) and collected into low-binding 1.5 ml Eppendorf tubes pre-coated with 2% FCS-PBS to reduce nuclei clumping and aggregation. Next, nuclei were concentrated by centrifugation, and their quality and concentration were established manually with hemocytometer, and processed immediately to the single cell workflow.

Single nuclei workflow

Single nuclei RNA-seq was performed using 10x Next GEM Single Cell 3 GEM kit v3.1 (10x Genomics; Pleasanton, CA, USA) according to the manufacturers protocol. Separate 10x genomics reactions were used for each sample. Generated libraries were sequenced on an Illumina NovaSeq with >27.5 x 10^3 reads per cell followed by de-multiplexing and mapping to the domesticated pig genome (build Sscrofa11.1) using CellRanger v5.0.1 (10x Genomics).

Bioinformatics analyses

Data pre-processing

Gene expression matrices were generated using the Cell Ranger software v5.0.1 (10x Genomics) with standard settings and mapping to the Sscrofa11 reference pig genome. The following data analysis was performed using Seurat package v5.0.[91] Firstly, we performed data filtering steps by removing low expressed genes and low-quality nuclei from further analyses: (i) genes with 0 raw counts were removed; (ii) nuclei with <500 or >6000 uniquely expressed genes, or with >25000 UMIs were excluded; (iii) nuclei with high percentage of mitochondrial genes (>5%) were removed. Next, the data were corrected for ambient RNA with SoupX using automated contamination estimation method.[92] The data were normalized using the *NormalizeData()* function, the 1500 most variable features detected with *FindVariableFeatures()*, data scaled with *ScaleData()*, the first 11 principal components calculated with *RunPCA()*, and used for clustering (*RunUMAP(), FindNeighbours(), FindClusters()*). Doublets were removed with the DoubletFinder package according to the doublet rates provided by 10x Genomics.[93] Next, we integrated the data from all samples into one object with Harmony[94] using first 11 principal components, and annotated major cell types. Clusters were annotated based on the expression of canonical markers[37,39,61]: *PECAM1* (*CD31*) and *CDH5* (ECs); *POSTN*, *DCN, PDGFRA* (FBs); *MYH11, COL13A1* (SMC); *PDGFRB, RGS6, CTNNA3* (pericytes); *PLP1, GRIK3* (Schwann cells); *SPON1, KCNIP1* (stromal cells); *PTPRC, FMN1, CD163, DOCK4* (myeloid cells); *BCL11B, IKZF1, SKAP1, NKG7, PAX5, CD8A* (lymphoid cells); as well as unbiased markers identified by *FindAllMarkers()* function. For further analyses, cells were separated according to their cell type (SMC, EC, myeloid, lymphoid) for sub-clustering and differential gene expression analysis. For immune cells ScType[95] R package was used for cell type prediction, followed by manual curation based on the gene module score enrichment. Module scores were calculated per each cell using *AddModuleScore()* function, following genes were used to assign the modules: arterial (intima) ECs (*FBLN5, HEY1, SEMA3G, ID1, SLC9A3R2, GJA4, GJA5, DKK2, SERPINE2*); Vasa vasorum ECs (*NR2F2, VWF, RGCC, CA4, ACKR1, FABP4, PLVAP*); TGFβ signaling (*KLF11, TGFB2, DAB2, CAV1, RAF1, SMAD6, SKIL, SMAD7, ACVRL1, BMP2, ID1, SMURF1, ACVR1B, HDAC1, SMAD2, ROCK1, AMHR2*); Chemotaxis (*PLAT, SELP, ICAM1, VCAM1, ACKR1, CEMIP2, ITGA6*); Resident-like MF (*CD163, LYVE1, LGMN, MARCO, FOLR2, F13A1, SELENOP, MRC1, TIMD4, CXCR1, CXCR4, SECISBP2L*); Inflammatory MF (*CD74, CD83, CD80, CD86, KDM6B, HLA-DRA, TNF, IL1, CXCL2, NFKBIA, NLRP3, CCL2, CCL3, CCL4, CCL5, CD68*); Foamy MF

(*TREM2, ABCA1, FABP4, CYP7A1, LIPA, SLC9B2, CD9, MREG, PPARG, ACAT1, APOE, ABCG1, OLR1, NPC1, NPC2, NR1H2, NR1H3, SCARB1*); SMC-like (*MYH11, ACTA2, COL1A1, MYH9); Progenitor-like MF (KIT, CD34, THY1, CD38, FLT3, CD93, SLAMF1*). Markers used for T-cell subcluster identification: *CD4, CD8A; FOXP3, IL2RA, LEF1, SELL, IL7R* – regulatory/memory T-cells; *NKG7, GZMH, GZMA, GZMK, PRF1* – cytotoxic T-cells.[43] Differentially expressed genes (DEGs) were obtained using the *FindMarkers()* function based on the non-parametric Wilcoxon rank sum test with Benjamini p-value correction. Significant DEGs were identified by the criteria Benjamini-adjusted p-value (p-adj) < 0.05.

Heatmaps

Heatmaps were generated using log2(FC) of DEGs, or z-scores calculated for average expression per cluster as indicated in Fig. legends via the *ggplot2* R package. For better visual representation, upper and lower value cut-offs were introduced as stated on the heatmaps. Genes used for heatmaps were derived from the BioPlanet 2019 or KEGG Human 2021 databases.

GSEA, GO and pathway enrichment analysis

Gene set enrichment analysis (GSEA) was performed using *ClusterProfiler*[96] R package using *gseGO()* function and human Ensemble database. Analyses was done on DEG lists ranked by the log2FC. Gene ontology (GO) and pathway enrichment analyses were performed using *Enrichr*,[97] with BioPlanet 2019 or KEGG Human 2021 databases. Selected pathways and GO-terms significantly enriched with a Benjamini-adjusted P-value (P-adj) < 0.05 are presented. Data are presented on a $-\log_{10}$ scale.

Cell-cell interaction network analysis

Cell-cell interaction network analysis was performed on all cell types for control and atherosclerosis conditions separately using CellChat R package.[46] Interactions were inferred based on the human ligand-receptor database Cell.ChatDB.human using the following parameters: *computeCommunProb*(cellchat, type = "triMean", population.size = TRUE), taking into account the scaling for the cell type population size. Cell-cell communications with clusters of nuclei less than 30 were filtered out by function *filterCommunication*(cellchat, min.cells = 30). Word clouds were generated with *computeEnrichmentScore()* function using all interactions in control and atherosclerosis conditions respectively. Differential interactions between control and atherosclerosis condition were calculated using *identifyOverExpressedGenes()* function with following parameters: thresh.pc = 0.1, thresh.fc = 0.05, thresh.p = 0.05, group.DE.combined = FALSE, only.pos = FALSE.

Comparison with human and mouse studies

For comparison of changes occurred in atherosclerosis vs. control condition in pig with the human and mouse datasets, we utilized publicly available bulk and single cell transcriptomic data.[37,39,55–59]

To correlate of DEGs in atherosclerosis vs. control condition in pig with the human and mouse datasets, we used the datasets, which contain both disease and control condition samples.[55,58,59] We re-analyzed scRNA-seq data as mentioned above in **Data pre-pocessing**, and generated DEG lists by Seurat *FindMarkers()* on major cell type populations: SMCs, ECs, and FBs. For human bulk RNA-seq data,[59] we used the DEGs provided by the authors for the comparison of abdominal aorta plaques to the left internal mammary artery controls. Only the genes with (1) direct orthologs, (2) a Benjamini-adjusted P-value (P-adj) < 0.001, and (3) with absolute log2 fold change >1, were considered for analysis using Pearson correlation test.

To compare the atherosclerotic plaque heterogeneity and cell subtypes in pig and human, we integrated several human datasets of containing samples from carotid, coronary, and aortic vessels.[37,39,55–57] We re-analyzed scRNA-seq data as mentioned above in **Data pre-pocessing**, and integrated datasets using Harmony integration. Cell types and subtypes were annotated according to the gene module score enrichment of top 100 markers per cluster of integrated data provided elsewhere[39] using *AddModuleScore()* function. For comparison between cell subtypes, single cell objects containing only SMCs, ECs, or immune cells were subset in both pig and human cases. Cluster similarity was determined using *clusterFoldSimilarity()* function of ClusterFoldSimilarity R package,[98] where the similarity values were based on the fold-changes from non-integrated pig and human datasets per each cluster computed using a Bayesian approach with fold-change shrinkage. Similarity heatmaps were generated using *similarityHeatmap()* function.

QUANTIFICATION AND STATISTICAL ANALYSIS

Data, which were not derived from sc/snRNA-seq data analyses, are provided as mean ± standard error of the mean (SEM). All statistical tests were exclusively undertaken on biological replicates using GraphPad Prism 10 software and or R. Comparison of data between the indicated two groups was undertaken using the non-parametric Mann-Whitney test, unless otherwise specified. Comparison of cell percentages per cell type/subtype in snRNA-seq data was performed using Chi-squared test. A p-value < 0.05 was considered statistically significant; * indicates p-values < 0.05, ** < 0.01, *** < 0.001, **** < 0.0001.